Aerospace Science and Technology 177 (2026) 112734

Contents lists available at ScienceDirect

Aerospace Science and Technology

journal homepage: www.elsevier.com/locate/aescte

Multidisciplinary design optimization of distributed electric propulsion aircraft with trim and flying qualities constraints using surrogate models

D. Granata [a], S. Mancini [b], A. Mateo-Gabin [c], A. Zanotti [a,*]

[a] Politecnico di Milano, Dipartimento di Scienze e Tecnologie Aerospaziali, via La Masa 34, 20156, Milan, Italy
[b] Airbus Defence and Space GmbH, Rechliner Str., Manching, 85077, Germany
[c] Airbus Defence and Space SAU, Paseo John Lennon, Getafe, 28906, Spain

ARTICLE INFO

Communicated by Dr Yu Lv

Keywords:
Multidisciplinary design optimization
Distributed electric propulsion
Aerodynamics
Surrogate modelling
Machine learning
Flying qualities

ABSTRACT

Hybrid-electric regional aircraft characterized by distributed electric propulsion offer promising benefits but introduce strong couplings problems between aerodynamics, structures, propulsion, and power systems, requiring a multidisciplinary design and optimization (MDO) approach to capture relevant trade-offs. This work presents an extended MDO framework applied to the Clean Aviation HERA configuration, developed within a collaboration between Politecnico di Milano and Airbus Defence and Space. The framework enhances traditional aerostructural optimization considering the use of the aerodynamic solver DUST, based on Vortex Particle Method (VPM) and by explicitly incorporating stability, control, and automatic trim requirements as design constraints. To limit the computational cost of aerodynamic simulations, surrogate models based on supervised machine learning regression and design of experiments (DOE) are employed within a multi-fidelity strategy. Results show consistent performance improvements in trimmed flight conditions, with successful enforcement of stability and flying qualities constraints. Furthermore, comparison between surrogate-based and high-fidelity optimizations highlights both the accuracy of the reduced-order models and their effectiveness in lowering computational costs.

1. Introduction

Technological development in the aerospace sector is increasingly being driven by environmental goals. Indeed, along with new architectural solutions, substantial effort goes toward refining conventional systems so they keep or improve performance while lowering enviromental impact.

At smaller scales, Urban Air Mobility (UAM) aircraft under development in the recent years responds directly to congestion, pollution, and dense populations. Indeed, electric vertical take-off and landing (eVTOL) aircraft promise fast, efficient urban and regional links thanks to electric propulsion, advances in energy storage and lighter materials [1]. Despite their operational potentiality, eVTOLs must still solve crucial problems, such as noise and acoustic impact, certification and safety frameworks, and the roll-out of vertiports and charging/refueling infrastructure. At the larger commercial scale, programs like Airbus's ZEROe investigate hydrogen and other fuels to decarbonize air travel [2], demonstrating that both evolutionary improvements and radical concepts are needed to meet international sustainability targets. In regional aviation, the push to cut emissions while ensuring high performance has also gained considerable importance. As part of the Clean Aviation program, the Hybrid-Electric Regional Architecture (HERA) project [3] has been launched to explore and refine aircraft concepts that integrate hybrid-electric propulsion. The objective is to define viable configurations capable of achieving the 50% reduction in greenhouse gas (GHG) emissions set out in the Strategic Research and Innovation Agenda (SRIA). Designed for 50-100 passengers and ranges of up to 1000 km, the aircraft is targeted for entry into service in the 2040s. It will be conceived as a component of multimodal transport networks and will employ hybrid-electric systems powered by batteries or fuel cells in combination with Sustainable Aviation Fuels (SAF) or hydrogen combustion. Such an approach is projected to deliver emission cuts of up to 90% while remaining fully compliant with ICAO noise standards. Fig. 1 shows a conceptual representation of HERA aircraft.

A key characteristic under investigation in the HERA project is the use of distributed electric propulsion (DEP), where several propellers powered by hybrid or electric systems are positioned along the wing span. This configuration increases safety by ensuring propulsion redundancy and at the same time has the potential to influence the aerodynamic behavior of the aircraft [4]. The mutual interaction between propellers and wing strongly affects lift generation and overall efficiency, while also making the design particularly sensitive to parameters linked

* Corresponding author.
E-mail address: alex.zanotti@polimi.it (A. Zanotti).

https://doi.org/10.1016/j.ast.2026.112734
Received 8 January 2026; Received in revised form 29 May 2026; Accepted 29 May 2026
Available online 1 June 2026

Notation

Symbol	Description
A_{cap}	wing caps area
$A_{stringer}$	wing stringers area
b	wing semi-span
c	wing chord @root
$\bar{c}$	wing mean chord
c_s	specific fuel consumption
C_j	aerodynamic coefficient
C_l	sectional lift coefficient
C_m	pitching moment coefficient
C_p	pressure coefficient
C_X	X-force coefficient
C_Z	Z-force coefficient
D	Aircraft integral Drag
f	objective function
F_X	X-Force in body axes
F_Z	Z-Force in body axes
g	constraint expression
L	aircraft integral Lift
$\vec{m}_{vec}$	aircraft mass vector (mass, CG and inertia)
m_{wing}	wing mass
m_Y	pitching moment in body axes
q	pitch rate
R	aircraft range
R^2	coefficient of determination
R_e	regressor relative error
RFC	reserve factor in compression
RFT	reserve factor in tension
$RMSE$	Root Mean Square Error
$S.M.$	aircraft static stability margin
U	Freestream velocity
V_Z	flowfield velocity Z-component in aircraft axes
W	aircraft weight
x_i	i-th design variable
x_{CG}	aircraft center of gravity long. coordinate
x_{NP}	aircraft neutral point long. coordinate
y_{kink}	wing kink y-coordinate
y_{eprop}	wing electric propellers y-coordinate
α	angle of attack
δ_e	elevator angle position
$\theta_{electric}$	electric rotor blade pitch angle
θ_{hybrid}	hybrid rotor pitch angle
ω_{sp}	aircraft short period mode frequency
ζ_{sp}	aircraft short period mode damping
ζ_{ph}	aircraft phugoid mode damping

to propeller geometry [5]. Although distributed propulsion can offer relevant performance advantages, it simultaneously presents complex engineering challenges that must be overcome [6].

A wide effort in literature has demonstrated that aerodynamic interactions between propellers and wings, as well as between multiple propellers, play a crucial role in determining the performance of novel aircraft configurations and are highly sensitive to design variables. These effects manifest through phenomena such as rotor-induced downwash, local variations in dynamic pressure, and the presence of upwash and downwash regions depending on the direction of rotation. Such mechanisms can considerably modify the load distribution on the wing, while the wing itself generates thickness and doublet-induced velocities on the propeller disk [7]. Recently, both experimental campaigns and numerical analyses were performed at Politecnico di Milano to quantify these effects and to assess their dependence on different geometric and operational parameters [8–10]. Similar investigations were conducted by

Fig. 1. HERA conceptual design representation.

Qiao and Barakos [11], who analyzed distributed and wingtip-mounted propellers using the HMB3 CFD solver, showing that these aerodynamic couplings systematically affect the efficiency of both the wing and the propellers, and leaving room in the design space for improvement of the configuration. In addition to these aerodynamic aspects, distributed propulsion introduces unsteady loading conditions that may reduce passenger comfort and lead into instabilities, thus extending the problem into a multidisciplinary domain [12].

For this reasons, hybrid-electric configurations like HERA require a highly multidisciplinary design approach from the earliest stages of development. This includes not only aerodynamic and structural aspects [13], but also propulsion, acoustics, and safety certification requirements [14]. One of the main strengths of a multidisciplinary approach is indeed the possibility to optimize design objectives that arise from individual disciplines, for example the aerodynamic lift-to-drag ratio or the wing's structural mass [15]. These metrics are directly tied to operating and manufacturing costs, and thus to the economic viability of the aircraft. The interdependencies that characterize hybrid-electric DEP architectures are more intricate than in conventional configurations, making coordinated optimization across disciplines a prerequisite for feasible and competitive solutions [16].

Affordability is also heavily conditioned by certification and social acceptance. Certification represents one of the most resource-intensive stages of aircraft development, with strict safety requirements often forcing repeated testing, validation campaigns, and redesigns in response to regulatory feedback. This iterative process can significantly increase costs and delay entry into service. For this reason, including certification-related constraints such as flying qualities requirements in the earliest design phases can substantially improve overall feasibility.

Because of the broad range of strongly coupled variables characterizing advanced aircraft concepts, multidisciplinary design and optimization (MDO) has become a widely adopted methodology in both conceptual and preliminary design phases [17–19]. Several studies have shown how MDO frameworks can support the management of subsystem interactions and trade-offs. Hendricks et al. [20] presented an MDO formulation for preliminary eVTOL design, highlighting the role of subsystem coupling, while Petersson et al. [21] discussed the benefits of early constraint integration in industrial design processes. Gazaix et al. [22] addressed aero-structural optimization problems, pointing out the challenges associated with higher-fidelity load predictions.

In the context of distributed electric propulsion (DEP) aircraft, many existing optimization and MDO studies primarily address aerodynamic and propulsive performance, whereas trim, stability, and control aspects are often treated separately or not explicitly included in the optimization loop. Several works investigate aerodynamic optimization of DEP-equipped wings using sequential or decoupled approaches. For example, Wu et al. [5] considers wing and propeller geometries independently,

while [23] explores the design space by varying the number of propellers and constraint sets. In these studies, objectives are generally limited to aerodynamic performance in cruise and take-off conditions, without explicitly accounting for aircraft trim or overall weight-and-balance consistency.

Other contributions extend the analysis to multiple mission profiles and configurations. In [24], aerodynamic optimization results are reported for several DEP configurations, but trim conditions and comprehensive weight-and-balance models are not included within the loop. Similarly, Biser et al. [25] proposes a multidisciplinary optimization framework for a regional aircraft concept, with a primary focus on drivetrain sizing. In that work, aerodynamics is analyzed separately using a combination of actuator-disk CFD models and simplified reduced-order models, while trim and flight mechanics analyses are conducted outside the optimization loop, despite their coupling with stability characteristics.

More integrated approaches have also been proposed. An MDO framework based on low-fidelity aerodynamic tools and reduced-order models is presented in [26], including a weight-and-balance model and basic trim and static margin constraints to minimize energy consumption over a mission profile. While this represents progress toward integration, the aerodynamic fidelity and the treatment of stability and control remain limited. A further step in aerodynamic modelling for preliminary design is reported by Granata et al. [27], who employed the mid-fidelity aerodynamic solver DUST to reconstruct stability derivatives through simulations of oscillatory motions. This capability allows flight mechanics modeling and the consideration of flying qualities at the preliminary design stage, as discussed in [28], but these analyses are not embedded within an optimization loop.

To manage computational costs, surrogate and reduced-order models have been adopted in several contexts. Frink et al. [29] used Kriging-based surrogate models to approximate the aerodynamic response of the SACCON configuration, reducing computational effort while retaining accuracy. However, in most DEP-related MDO studies, surrogate models are developed for specific applications and are not systematically integrated as interchangeable elements within a unified framework.

Within this context, the present work extends existing DEP-oriented MDO approaches by integrating trim, stability, and control evaluations directly within the optimization loop. The trim condition is solved automatically for each candidate design, ensuring that performance is assessed at the corresponding equilibrium state, in contrast with most previous studies where trim is neglected or enforced through simplified constraints. The inclusion of static and dynamic stability constraints, such as short-period and phugoid modes, enables flying qualities to be considered already at the preliminary design stage, which is particularly important for innovative configurations whose stability characteristics may differ from those of conventional aircraft. The focus is therefore on the implementation of a methodology that allows these constraints to be enforced automatically within the MDO process.

These analyses are enabled by the use of the mid-fidelity aerodynamic solver DUST, which provides automated routines for stability and control assessment and captures aerodynamic interaction effects that are fundamental for DEP configurations and cannot be reliably represented by lower-fidelity aerodynamic models. In addition, the work adopts a structured approach to surrogate modeling within the MDO framework, where aerodynamic and stability-and-control disciplines are represented both through physics-based solvers and through supervised machine-learning surrogates trained using systematic design-of-experiments strategies. Compared to existing applications, in which surrogate models are often introduced in an ad hoc manner, the present framework allows surrogate and full-order models to be used consistently and interchangeably within the optimization process, while preserving the accuracy of the mid-fidelity analyses and reducing computational cost.

Overall, the contribution of this work lies in the extension of existing MDO frameworks to include automated trim and stability assessments together with a consistent surrogate-based strategy, enabling a more comprehensive and practically relevant preliminary design exploration for DEP aircraft while retaining the underlying physics of stability and control through the modeling of aerodynamic interaction effects enabled by the mid-fidelity solver DUST.

2. Numerical methodology

The developed framework leverages on the use of the aerodynamic solver DUST [30] and of the optimizer GEMSEO [31].

2.1. DUST

DUST is a mid-fidelity aerodynamic computational tool, developed by Politecnico di Milano, which provides a fast and reliable simulation environment for complex aircraft configurations, such as eVTOL aircraft, tiltrotors and DEP configurations. DUST is an open-source code released under the MIT license, integrating different aerodynamic models for solid bodies, thick surface panels, thin vortex lattice elements, and lifting line elements. Additionally, a Vortex Particle Method (VPM) is implemented for wake modeling, offering a stable Lagrangian representation of free-vorticity flow fields. This feature makes it particularly suitable for numerical simulations of configurations with strong aerodynamic interactions. Details regarding the solver's mathematical formulation can be found in [32]. In this study, DUST is used to develop the aerodynamic model of the HERA aircraft and to perform aerodynamic analyses, including polar curves, stability and control assessments, and wake interaction aerodynamics studies.

2.2. GEMSEO

GEMSEO (Generic Engine for Multidisciplinary Scenarios, Exploration, and Optimization) is an open-source Python-based software designed to automate multidisciplinary processes, particularly those related to Multidisciplinary Design Optimization (MDO). It offers a variety of MDO formulations and is built on NumPy, SciPy, and Matplotlib, incorporating algorithms for coupling, design of experiments, linear problems, optimization, machine learning, surrogate modeling, uncertainty quantification, and visualization. GEMSEO can be integrated into simulation platforms or used as a standalone tool. It supports Python, MATLAB, Scilab scripts, Excel spreadsheets, and other executable codes callable from Python.

2.3. HERA aerodynamic numerical model

In this work, the aerodynamic model of the HERA aircraft developed in DUST is presented and validated against RANS simulations performed using TAU solver with Spalart-Allmaras turbulence model [33]. DUST was employed to estimate aerodynamic loads, assess stability, and evaluate flying qualities. A simplified vortex-lattice version of the model was also integrated into the MDO loop for configuration optimization.

HERA configuration includes a main wing, a T-tail, and a hybrid-electric propulsion system with one hybrid rotor near each wing root and two smaller electric rotors farther outboard, with thrust distribution varying by flight regime. Fig. 2 shows DUST aerodynamic model, composed by a total number of 14,460 mesh elements, and the reference frame employed to evaluate the loads in body and wind axes. The main lifting surfaces were fully parameterized and modeled with surface panel (SP) elements, while control surfaces were added using DUST's built-in tools as described in [34]. The fuselage mesh was generated following [35]. A reduced model of the lifting surfaces was also built by substituting surface panels with vortex-lattice (VL) elements to be used along with the optimization, as enabling to achieve up to a 10x reduction in computational cost. Rotors were modeled using lifting-line elements [32] using two-dimensional airfoils aerodynamic coefficients

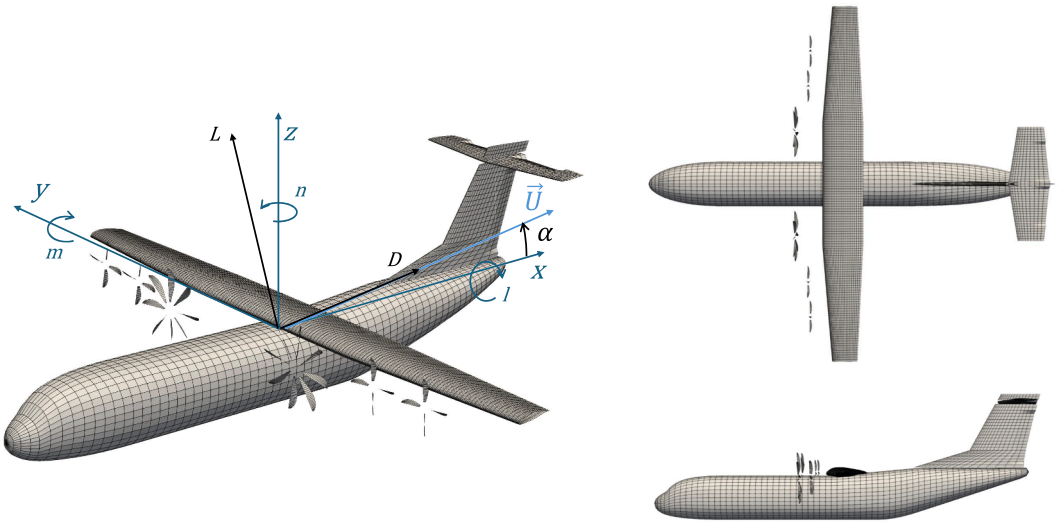

Fig. 2. HERA DUST aerodynamic mesh and body axes orientation.

Table 1
Aerodynamic mesh specifications (Vortex Lattice model in brackets).

Solver	N.Components	N.elements x comp.
Wing	1	9000 (600)
Tail	1	2080 (400)
Hybrid Rotor	2	232 (144)
Electric Rotor	4	116 (72)
Fuselage	1	2452 (/)
Total	/	14,460 (1216)

tables generated via NeuralFoil [36]. Parasite drag, not accurately captured by the mid-fidelity solver due the intrinsic limitations of potential methods, was considered in the load evaluation for the optimization as an added constant value calculated from preliminary CFD analyses performed using TAU. The presented mid-fidelity model does not capture viscous flow separation effects occurring at high angles of attack due to the limitation of the implemented potential approach and is therefore applicable only within the pre-stall aerodynamic regime. To address this limitation, throughout the following study, the trim angle of attack variable is constrained to remain within the admissible pre-stall range, which is estimated through high-fidelity CFD analyses, as will be discussed in Section 3.1.

Table 1 summarizes the number of mesh elements for each component of the aerodynamic model, including both the surface panel model and the reduced vortex-lattice versions. The mesh was defined based on a convergence study for each component, that has ensured load variations below 0.5%. Steady-state aerodynamic simulations, used for both validation and evaluation of the aircraft's static stability, were performed using a total simulation time of 0.3 s and a time step of 0.001 s. On the other hand, to calculate dynamic derivatives, the total time of the dynamic simulations was increased to 1 s, as done in [27]. For optimization purposes, only cruise flight conditions are considered.

2.4. Multidisciplinary optimization framework

This section describes the multidisciplinary optimization (MDO) environment employed for the present work. The framwork has been developed in previous works [37,38] at Airbus Defence and Space, and it has been extended and refined in this study to meet the objectives introduced in the previous section. This section details the environment's structure, implementation logic, and the new features added in the present work.

The MDO framework couples multiple disciplines representing key flight physics aspects of the aircraft. It is built around the open-source optimizer GEMSEO [31], which is designed for multidisciplinary coupling and data exchange. A custom library manages communication among design variables associated with different aircraft components. The overall framework consists of several modules interfaced with GEMSEO, coordinated by an executable script that defines the optimization logic and allows the user to select from various optimization strategies available within GEMSEO.

The assembly module serves as a descriptive layer linking the flight environment (mission segment or flight condition) with the aircraft's physical components. It contains all classes defining subsystems, implemented as objects with attributes (properties) and methods (operations). For instance, the *Section* class stores data for each airfoil profile within the parametric *Wing* class. The subsystem interconnections follow the CPACS convention [39], ensuring proper management of interaction constraints (e.g., geometric dependencies). Simple elements are combined hierarchically to form the complete system. Complex components, such as a propeller that consists of multiple identical blades each defined by sectional properties, maintain the relevant data at their respective levels (Fig. 3).

Discipline modules represent independent physical models (e.g. aerodynamics, structure, etc) integrated into GEMSEO through dedicated interfaces specifying required inputs and generated outputs. Each discipline module retrieves data from the assembly and produces standardized outputs that can be used as objectives or constraints during optimization. The disciplines developed in the present work focus on the aero-structural optimization of HERA's main wing, while ensuring compliance with flying qualities constraints, as described in the following.

Aerodynamics: discipline interfaces with the mid-fidelity solver DUST, using inputs from the assembly to define geometry and flight conditions. It allows user control over parameters such as timestep, total simulated time, mesh resolution, wake panels, and vortex particles. In addition to static analyses, it computes static and dynamic stability derivatives (following the formulation described in [27] formulation),

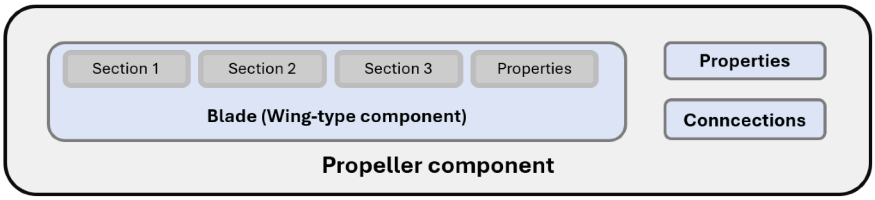

Fig. 3. Data structure of a propeller component.

and control derivatives (aileron, elevator, rudder) via finite differences. Outputs include aerodynamic loads and all relevant stability/control (S&C) derivatives.

Structural Sizing: The structural discipline sizes the primary wing structure, while fuselage and tail structures are kept fixed in terms of mass per unit area. Fuselage is also kept constant in terms of geometry, while the tail vary its weight proportionally to its surface, as done in [40]. Fuselage geometry and structure were excluded from the design variables based on two main engineering considerations. Indeed, lifting surface modifications have a negligible impact on the fuselage preliminary structure design, and the overall flight mechanics and stability remain predominantly driven by the wings and tail. Additionally, keeping the fuselage fixed avoids possible misleading design trends, due to the mid-fidelity nature of DUST model that cannot accurately capture viscous effects around bluff bodies. Regarding the wing, the structural sizing discipline determines the thickness distribution of skins, spars, stringers, and ribs based on spanwise aerodynamic loads and engine mass data, enforcing a reserve factor (RF) of 1.5. The sizing is performed using Airbus's in-house tool AMPET [41], integrated within the GEMSEO-based MDO framework [42]. The wing primary structure accounts for approximately 85% of the total wing mass, excluding fuel and engine masses, which are provided as inputs to the structural analysis. When the wing structure is properly sized, the resulting wing mass can therefore be predicted with limited uncertainty, making the accuracy of the aerodynamic loads a key aspect of the optimization. Structural sizing accounts for spanwise distributions of forces and moments from the aerodynamic discipline, together with engine weights and locations, the wing-fuselage attachment position, and flight conditions relevant to bird strike requirements on the leading edge. The wing structural concept is defined through material properties, spar locations, stringer spacing on the upper and lower skins, and rib number and spacing. In this work, aerodynamic loads are provided directly by the DUST solver, which computes consistent spanwise force and moment distributions including wing-propeller interaction effects characteristic of distributed electric propulsion configurations. These loads are transferred without simplification to AMPET, ensuring a physically consistent aero-structural coupling within the MDO loop. Given the applied loads and initial sectional definitions of caps and stringers, AMPET evaluates stresses in skins and spar webs due to external loads, secondary effects such as Brazier loads, and shear and bending contributions. For each wing section, the tool determines the minimum-weight thickness distribution satisfying von Mises stress limits, buckling constraints based on Timoshenko and Gere theory, combined criteria for spar webs, and bird strike requirements, while maintaining RF = 1.5. Manufacturing constraints are enforced by restricting thicknesses to manufacturable increments and limiting thickness variations between adjacent panels. After skins and spars are sized, ribs are dimensioned using the same criteria, and the resulting structural mass is computed from material properties and geometry and passed to the MDO framework, allowing aerodynamic interaction effects to be consistently reflected in the structural mass throughout the optimization. Fig. 4 shows a schematic representation of DUST-GEMSEO interface and optimization loop with Multidisciplinary Feasible (MDF) MDO formulation architecture. Further details about the structural sizing procedure and the communication with DUST can be found in [43] and [41].

Weight and Balance: discipline aggregates the mass properties of all components. Each aircraft component has an assigned mass, center of gravity, and inertia tensor, either predefined or provided by other disciplines. This module computes total mass, global CG, and overall inertia in body axes of the aircraft, feeding this information into the stability and control discipline.

Stability and Control: discipline combines aerodynamic derivatives and inertia data to compute the static margin (SM), flying qualities (FQ) metrics (following forumlation described in [44]), and maneuvering time estimates based on control inputs and damping stability derivatives. It delivers the key parameters required to assess aircraft handling and flying qualities.

The *Variable* class defines the optimization variables, marking component attributes to be controlled by the optimizer. Each variable includes a name, initial value, and optional bounds, and is attached directly to a component property for tracking during the optimization process. Within GEMSEO, several MDO formulations are available to couple multidisciplinary analysis (MDA) with optimization, including the Multidisciplinary Feasible (MDF) approach, which solves the coupled system at each iteration; the Individual Discipline Feasible (IDF) approach, which treats coupling variables as independent with added consistency constraints and the Bi-Level formulation, which separates disciplinary optimization from system-level coordination. Detail about each approach can be found in [31]. Fig. 4 illustrates a high-level overview of the optimization loop and interactions among the framework components, using the MDF algorithm.

2.5. Surrogate modelling

The presented problem involves multiple disciplines and, as with DUST, requires running simulations using dedicated solvers. During an optimization process, this becomes particularly demanding because simulations must be repeatedly executed while varying design parameters to compute the Jacobian matrix, which provides sensitivity information to the optimization algorithm (Fig. 4). This results in significant computational costs, especially since a finite difference approach must be used for DUST during optimization. To mitigate this issue, surrogate models built through Design of Experiment (DOE) approaches have proven highly effective, as supported by recent literature [45,46]. A surrogate model approximates a discipline as an explicit Multi-Input Multi-Output (MIMO) function of the design variables involved in the optimization [47].

In the present framework, surrogate models are generated through a five-step DOE methodology. The first step, planning, defines the discipline input/output structure, the design space, and any constraints. In the second step, sampling, a set of meaningful points within the design space is selected to serve as inputs for the discipline evaluation. GEMSEO provides multiple sampling strategies, including Full Factorial Sampling (FFS), Latin Hypercube Sampling (LHS), quasi-random sequences such as Sobol or Halton, and simpler Monte Carlo methods [31]. The third step, execution, involves running the disciplinary solver on each sampled point and storing the outputs. The fourth step, regression, builds the surrogate model by training a regression algorithm to approximate the relationship between design variables and outputs. Supported techniques include linear and polynomial

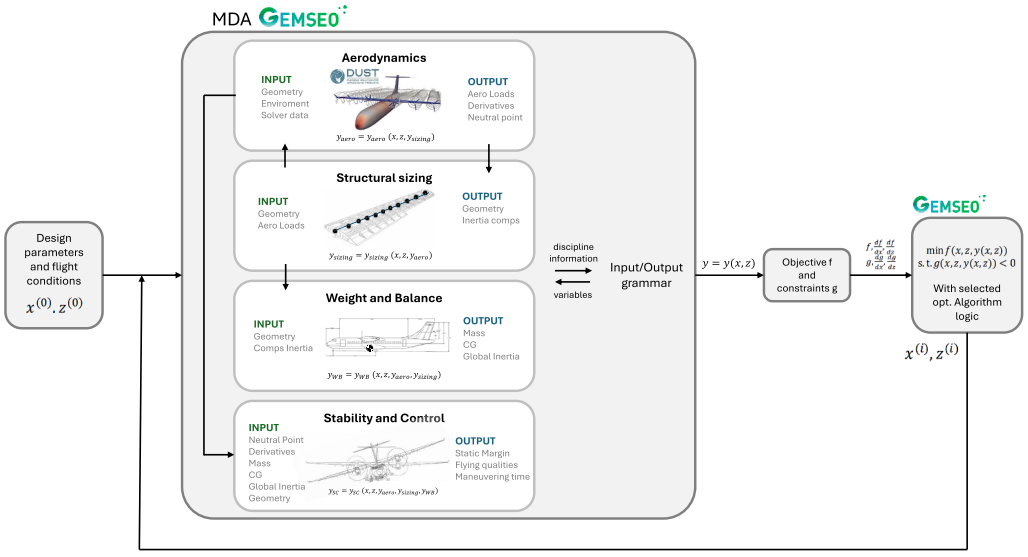

(a)

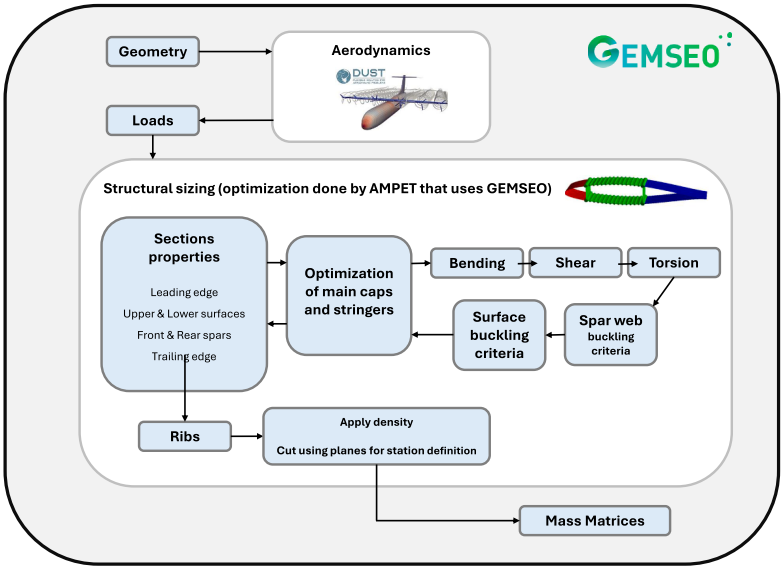

(b)

Fig. 4. (a) Schematic of DUST-GEMSEO interface and optimization loop with multidisciplinary feasible (MDF) MDO formulation architecture; (b) Zoom-in to the DUST-structural sizing (AMPET) internal coupling [16,41].

regression, Gaussian Process Regression (GPR), and Radial Basis Function (RBF) regressors, with GPR offering predictions and uncertainty estimates and RBF performing well for scattered nonlinear data. The final step, validation, assesses the model's accuracy by comparing its outputs with those of the original discipline. Validation points can be drawn from the sampling dataset or newly generated, and performance metrics such as the coefficient of determination (R^2), the relative error (R_e), or the Root Mean Square error ($RMSE$) are employed [31], and defined as

$$R^2 = 1 - \frac{\sum_i (\hat{y}_i - y_i)^2}{\sum_i (y_i - \bar{y})^2}, \quad R_e = \left| \frac{\hat{\mathbf{y}} - \mathbf{y}}{\mathbf{y}} \right|, \quad RMSE = \sqrt{\frac{1}{N} \sum_{i=1}^{N} \left(y_i - \hat{y}_i \right)^2} \tag{1}$$

where $\hat{\mathbf{y}}$ represents the model outputs at validation points, $\mathbf{y}$ represents the outputs of the original discipline, and N the number of training samples.

A dedicated module has been developed within the multidisciplinary framework to create surrogate models following this DOE approach. Each disciplinary block in Fig. 4 is treated as a black box with its own input/output structure, and GEMSEO's built-in algorithms are employed for sampling and model fitting. When the surrogate option is activated, the original block is replaced by a MIMO surrogate that preserves the same input/output structure, effectively replicating the behavior of the discipline with much lower computational effort.

In this work, the module was applied to create surrogate models for the aerodynamic loads and stability discipline, which relies on DUST (Fig. 4). Samples from DUST are selected using Latin Hypercube

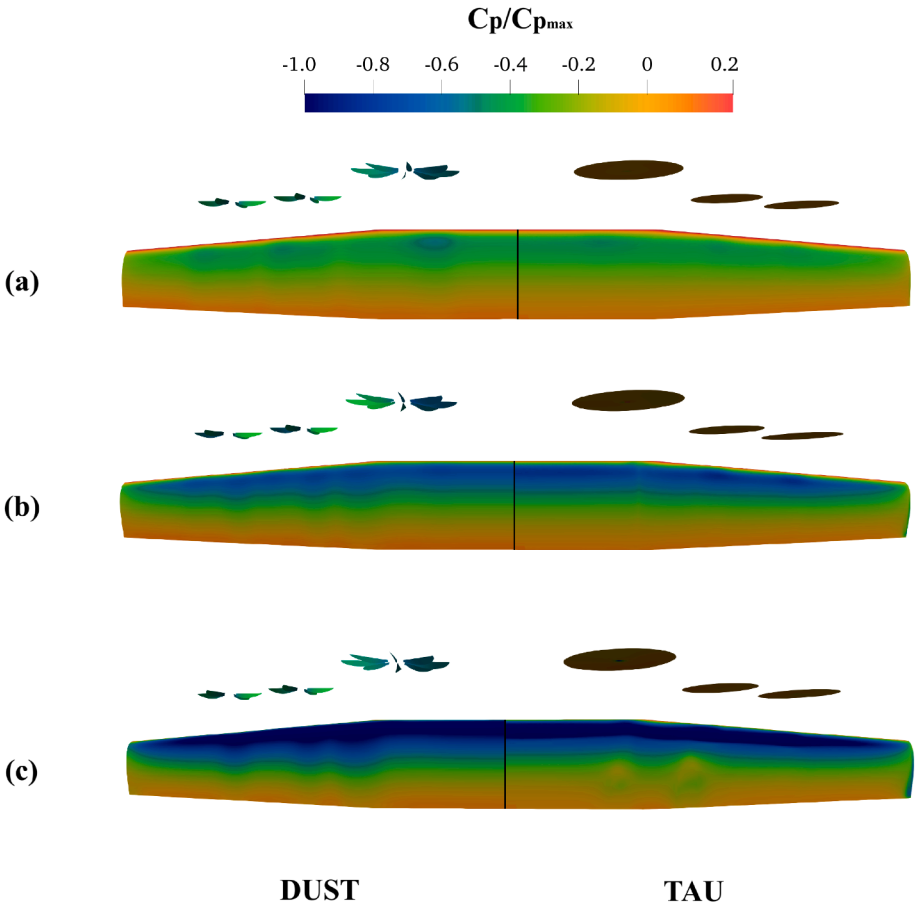

Fig. 5. Comparison of the pressure coefficient distribution on the wing between DUST and TAU (CFD RANS) solutions at (a) $\alpha = 0°$ (b) $\alpha = 5°$ (c) $\alpha = 10°$.

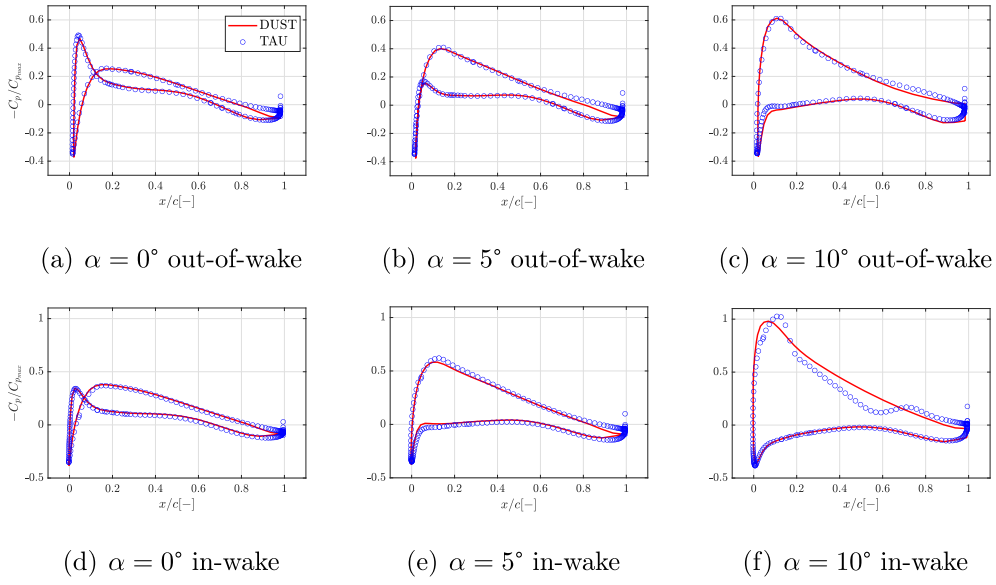

Fig. 6. Comparison of the chordwise sectional pressure coefficient distribution between DUST and TAU solutions, non-dimensionalized with respect to the maximum value, at different angles of attack, inside (in-wake: $y/b = 0.31$) and outside (out-of-wake: $y/b = 0.96$) the propeller wake.

Sampling (LHS) [48], which generates near-random points evenly distributed across the multidimensional parameter space. Surrogate models are then constructed from the DOE points using Gaussian Process Regression (GPR)[49] and Radial Basis Function (RBF) [50] regressors.

2.6. Methodology overview

The proposed methodology combines mid-fidelity aerodynamic modeling, surrogate-based acceleration, and integrated trim and

stability constraints within a unified MDO framework for DEP aircraft. The objective is to capture the key aerodynamic interaction effects typical of DEP configurations while maintaining computational efficiency compatible with iterative optimization and allowing the inclusion of constraints related to certification-relevant flying qualities. A preliminary aerodynamic analysis is first conducted to validate the DUST solver against high-fidelity RANS results obtained with the TAU solver. This validation focuses on both global aerodynamic coefficients and local load distributions, with particular attention to wing-propeller interaction effects that strongly influence loads, stability, and propulsive efficiency. Thanks to its vortex particle formulation DUST preserves vortical structures and interaction phenomena with a level of fidelity comparable to higher-fidelity CFD approaches, while avoiding the computational overhead associated with mesh refinement and large grid sizes. This makes DUST particularly suitable for optimization-driven studies where repeated aerodynamic evaluations are required. Once validated, DUST is used as the reference model for the generation of machine-learning-based surrogate models. This ensures consistency between high-fidelity CFD, mid-fidelity aerodynamics, and data-driven approximations, allowing the relevant physical trends to be retained across modeling levels. Surrogates are constructed using a systematic design-of-experiments approach with generic sampling strategies, and their accuracy is assessed through dedicated convergence studies with respect to training dataset size. Different regression techniques are evaluated, and the final surrogate models are selected based on accuracy and robustness criteria. Once trained, the surrogates are treated as interchangeable black-box replacements of the corresponding physics-based discipline models within the MDO framework. The optimization process is structured in two main phases. The first phase consists of an automatic trim optimization, in which force and moment equilibrium are solved within the loop to identify the steady-state cruise condition for each candidate configuration. The second phase addresses geometry and propeller placement optimization under trimmed cruise conditions, while enforcing constraints on static and dynamic stability as well as flying qualities. Stability derivatives and dynamic modes are computed directly using DUST-based aerodynamics, and all required routines are implemented within the framework, enabling the assessment of flying qualities metrics typically associated with certification requirements already at the preliminary design stage. Finally, the methodology includes a systematic comparison between optimization results obtained with full-order discipline models and those obtained using surrogate-based MDO. This comparison allows the deviation introduced by surrogate modeling to be quantified in terms of optimal design variables and objective function values, demonstrating the effectiveness of the surrogate strategy in reducing computational cost while preserving optimization accuracy. Although the present study focuses on the cruise condition to address the relevant aerodynamic and stability constraints, the proposed GEMSEO-based framework is inherently general and supports multi-scenario optimization [31], enabling consistent extension to multi-segments missions, as already done in [42].

3. Results and discussion

3.1. Aerodynamic analysis

This paragraph analyzes the cross-validation between DUST and TAU models, addressing the aerodynamic behaviour of the configuration. Fig. 5 shows a comparison of the pressure distribution between the DUST and TAU models. TAU CFD model includes actuator disks to represent the propellers tuned using thrust inputs from DUST modeling employing lifting line elements. The main goal of this activity is to determine the accuracy of DUST model in presence of possible viscous and non-linear effects occurring in the explored workspace. As shown in Fig. 5(a), at angle of attack $\alpha = 0^{\circ}$, the correlation between the two aerodynamic solvers is quite good, although the CFD solver, likely due to the use of actuator disks and mesh dissipation, exhibits a more limited interaction effect on the wing due to propellers. A similar observation can be made for Fig. 5(b), corresponding to $\alpha = 5^{\circ}$. At $\alpha = 10^{\circ}$, it is evident that DUST predicts stronger interaction effects, as seen from the larger spanwise deviation of pressure coefficient distribution (C_p). However, it fails to capture flow separation effects occurring at this higher angle of attack under cruise conditions. As will be shown later, this flow separation leads to a reduction of the wing aerodynamic loading that the VPM solver is not able to accurately reproduce at this higher attitude of the aircraft.

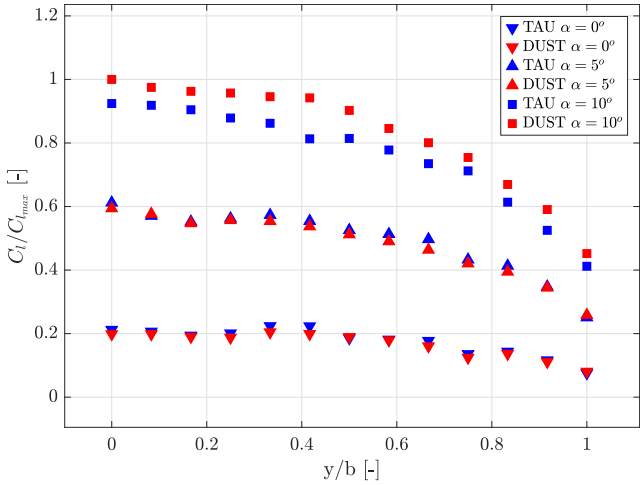

Fig. 7. Comparison of the sectional lift coefficient as a function of the wing spanwise coordinate between DUST and TAU solutions, at different angle of attacks.

Indeed, Fig. 6 shows the chordwise sectional distribution of C_p at angles of attack $\alpha = 0^{\circ}, 5^{\circ}, 10^{\circ}$, for two different spanwise sections, i.e. one located within the propeller wake (in-wake, $y/b = 0.2985$), and one outside the propeller wake (out-wake, $y/b = 0.9630$). It can be observed that for angles of attack $\alpha = 0^{\circ}$ and 5°, there is a quite good agreement between the mid- and high-fidelity models both on the in-wake and out-wake sections. However, for $\alpha = 10^{\circ}$, DUST accurately captures the behaviour of the sectional C_p in the out-wake section but higher discrepancies are found in the suction side of the in-wake section. This discrepancy is due to the fact that, in the in-wake wing region, the propeller wake induces an upwash and increases the dynamic pressure on the wing, triggering flow separation, as shown in Fig. 5. As can be observed more in details in Fig. 6(f), this flow separation manifests as a sudden drop in C_p, which results in a significant decrease of the wing loading in the wing in-wake region.

Fig. 7 shows the comparison between DUST and TAU in terms of the spanwise lift distribution at different angles of attack, i.e. $\alpha = 0, 5, 10^{\circ}$. A slight overestimation of the load by TAU compared to DUST can be observed, but overall the correlation is quite good at the lower two angles of attack, particularly in terms of the trend and the spanwise derivative of the load. At $\alpha = 10^{\circ}$, separation effects well captured by the CFD solver become significant, leading to noticeable differences in the load distribution. In fact, DUST overestimates the load by approximately 10%, highlighting the limitations of the VPM solver at higher angles of attack where incipient flow separation could occur.

Similar considerations apply to the integral loads in body axes shown in Fig. 8 in terms of vertical force coefficient C_Z, longitudinal force coefficient C_X, and pitching moment coefficient C_m (see definition in Fig. 2). In this representation, prior to the onset of stall at $\alpha = 10^{\circ}$, there is excellent agreement between the models, especially for the derivatives of C_{Z_α} and C_{m_α} calculated from DUST solution as the slope of the curves between 0° and 5°, which deviate by less than 1% from TAU results. These derivatives are crucial both for the computation of flying qualities (such as static margin and the frequencies and damping of the

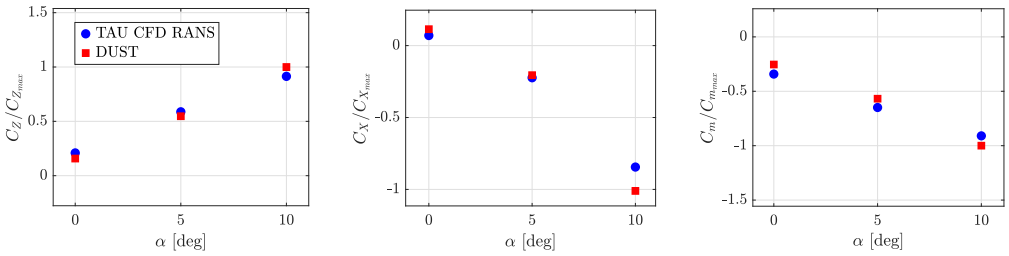

(a) Lift (b) Drag (c) Pitching Moment

Fig. 8. Comparison of integral loads coefficients between DUST and TAU as a function of the angle of attack.

aircraft flight mechanic modes) and for the gradient-based optimization process. Moreover, addressing the L/D ratio for the conditions tested, a deviation between DUST and TAU of less then 5% is observed.

Once the DUST model has been consistently validated against CFD results, a detailed analysis of the aerodynamic interaction effects influencing performance and, consequently, the optimization of a DEP configuration is presented. Fig. 9 shows the sectional blade loading coefficients of the hybrid-electric and fully electric propellers for different angles of attack, evaluated at 75% of the blade chord and expressed as a function of the blade azimuth angle ψ, representing the blade position over the revolution. The figure compares isolated rotor configurations with the coupled wing-rotor case, thereby highlighting the influence of the wing on rotor loading.

It can be observed that, consistently across all considered angles of attack and for all three propellers, the presence of the wing leads to an overall increase in blade loading. In addition, a pronounced first-harmonic (1/rev) component is introduced, whose amplitude increases with the angle of attack. This harmonic is associated with the variation of the effective inflow angle experienced by the rotor disk as the aircraft angle of attack increases. The observed behavior can be interpreted as the combined effect of wing-induced upwash and ground-effect-like aerodynamic interaction acting on the rotor blades, as discussed in more detail in [51].

Fig. 10 illustrates the complementary effect, namely the influence of the rotors on the wing. In particular, the induced velocity field generated by the lifting surfaces is evaluated at the wing leading edge, considering again a breakdown of configurations including the isolated wing ("*wing*"), the isolated rotors ("*rotors*"), and the coupled wing-propeller case ("*full*"). The visualization highlights both the spanwise location of the propellers and their direction of rotation relative to the wing span.

The results show that the rotor system induces a characteristic velocity dipole on the wing, which in turn produces a corresponding dipole in the local angle of attack [51]. This effect directly influences the spanwise load distribution, demonstrating the strong aerodynamic coupling between wing and propellers in DEP configurations.

Indeed, Fig. 11 presents a comparison between DUST solutions only, obtained using the surface panel and the vortex lattice models at different angles of attack. The effects of wing-propeller interaction on the spanwise loads can be clearly observed on both SP and VL models compared to the clean aircraft (w/o propellers) solution (shown by dashed curves), leading to a characteristic upwash-downwash dipole pattern in the induced velocity field. This results in local variations in angle of attack and loading when the propeller wake impinges on the wing. This phenomenon is consistently observed across all three angles of attack and leads to variations in the loads of up to 15%, highlighting the importance of accounting for aerodynamic interactions in the optimization process. The quite good correlation between the solutions obtained with the two models for lifting surfaces confirms that using vortex lattice representation enables to keep accuracy in capturing the physical interaction phenomena and the overall load trend behavior, while reducing substantially the computational effort. Thus, the VL model has been used along within the optimization process described in the following.

Table 2
Effect of Wing–Rotor interaction on aerodynamic L/D and thrust.

AoA [deg]	Configuration	L/D [-]	Δ L/D [%]	Δ Thrust [%]
0	Wing isolated	14.33	REF	–
	Rotors isolated	–	–	REF
	Wing + Rotors	16.24	+13.35	+11.21
5	Wing isolated	11.01	REF	–
	Rotors isolated	–	–	REF
	Wing + Rotors	12.20	+10.76	+12.12
10	Wing isolated	6.87	REF	–
	Rotors isolated	–	–	REF
	Wing + Rotors	7.15	+4.17	+5.73

Table 2 summarizes the effects of rotor-wing installation on aerodynamic loads and wing efficiency, highlighting variations of up to 15% associated with aerodynamic interaction effects. These results demonstrate the importance of accounting for such physical interactions within the modeling framework adopted for optimization purposes, as well as the potential to exploit them to maximize overall performance [5].

Fig. 12 highlights the capability of DUST modeling to capture wing-propeller interactions as shown by the visualization of the pressure coefficient (C_p) distribution over the wing, along with an iso-surface of vorticity based on the Q-criterion to represent the wake.

When considering the complete aircraft configuration, qualitative effects of wing-rotor interaction can again be observed on the wing pressure coefficient distribution, together with the influence of wing downwash on the horizontal tail, which results in a reduction of the tail pressure coefficient, as shown in Fig. 13. Fig. 14(a) and (b) present the integral load curves for the three configurations in terms of vertical force and pitching moment, respectively, while Fig. 14 reports the integrated loads acting on the horizontal tail alone for the same configurations.

By comparing Fig. 14(b) and (d), it is possible to both identify and quantify the stabilizing contribution of the horizontal tail, which shifts the integrated load curves toward lower pitching moments, and to assess the effect of wing-induced downwash on the tail loads. This effect is particularly relevant, as it directly influences the trim condition of the aircraft and, consequently, the wing angle of attack about which the optimization is performed within the MDO loop. The quantification of these effects in terms of the aircraft stability derivatives is reported in Table 3. A more extensive validation of DUST in capturing these interaction effects is provided in [52].

3.2. Trim optimization

This section addresses the longitudinal trim problem for the HERA aircraft configuration. The developed MDO framework is used to perform the trim, treating trim variables as design variables subject to constraints. Table 4 summarizes the problem definition. The trim variables

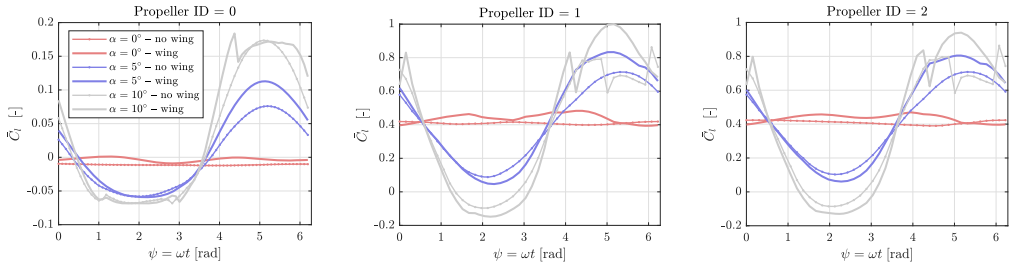

(a) Hybrid (b) Electric 1 (c) Electric 2

Fig. 9. Sectional blade loading coefficient of hybrid and electric rotors, for different angles of attack α, evaluated at 75% of the span (0.75 R), and expressed as a function of the azimuth angle ψ (Blade position over the revolution). Comparison between the rotor load with and without wing.

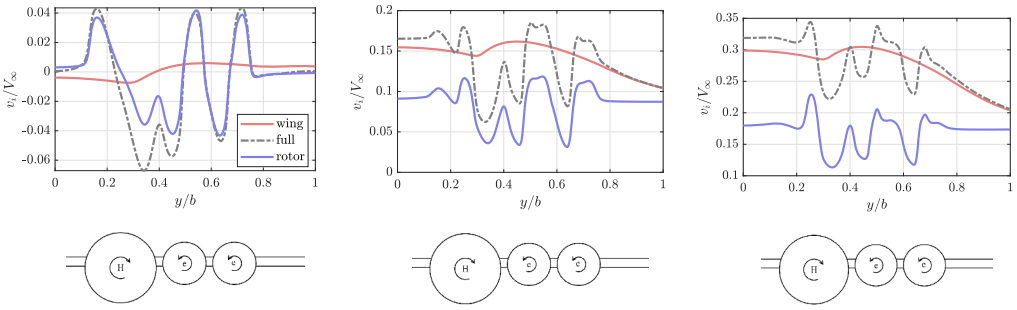

(a) $\alpha = 0°$ (b) $\alpha = 5°$ (c) $\alpha = 10°$

Fig. 10. Induced velocity at the wing leading edge, as a function of the wing span. Comparison for different angles of attack α and for the following cases: Full (wing + propeller), wing only, and rotors only.

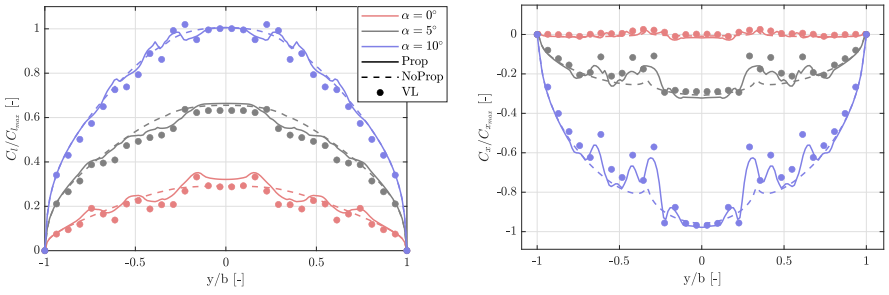

(a) (b)

Fig. 11. Comparison of (a) Spanwise wing sectional lift and (b) Axial force coefficient as a function of the spanwise coordinate for DUST Surface Panel (SP) and Vortex Lattice (VL) elements solutions. DUST solution for the clean aircraft without propellers is shown as dashed lines.

Table 3
Comparison of longitudinal aerodynamic derivatives and tail load variations.

Configuration	$\frac{\partial C_z}{\partial \alpha}$	$\Delta(\partial C_z/\partial\alpha)$ [%]	$\frac{\partial C_m}{\partial \alpha}$	$\Delta(\partial C_m/\partial\alpha)$ [%]	$\frac{\partial C_{z,\text{tail}}}{\partial \alpha}$	$\Delta(\partial C_{z,\text{tail}}/\partial\alpha)$ [%]	$\frac{\partial C_{m,\text{tail}}}{\partial \alpha}$	$\Delta(\partial C_{m,\text{tail}}/\partial\alpha)$ [%]
Full without rotors	0.065034	0.000	−0.041431	0.000	0.009575	0.000	−0.098089	0.000
Full with rotors	0.068198	4.865	−0.040348	2.614	0.010086	5.338	−0.103550	−5.569
Fuselage + tail	0.014139	−78.259	−0.091405	−120.620	0.011667	21.843	−0.120860	−23.217

include the aircraft angle of attack α, which primarily balances vertical forces ($\sum F_Z$), the blade pitch of the hybrid and electric motors $\theta_{hybrid}, \theta_{electric}$, which adjust rotor thrust to counteract drag and contribute to longitudinal force equilibrium ($\sum F_X$) and the elevator deflection δ_e, which mainly balances the pitching moment around the center of gravity ($\sum m_{Y_{CG}}$). The setup of the problem permits to obtain the optimal thrust split between the propellers. The angle-of-attack constraint accounts for the limitations of the mid-fidelity DUST model, which cannot capture viscous stall and flow separation occurring at high incidence. To ensure physical consistency, the trim optimization is restricted to the validated pre-stall operating region identified via high-fidelity CFD analyses.

Fig. 15 presents the Extended Design Structure Matrix (XDSM) for the trim problem, showing the inputs and outputs of each discipline and the optimization loop path highlighted in black. The trim optimization is performed using the SLSQP (Sequential Least Squares Programming)

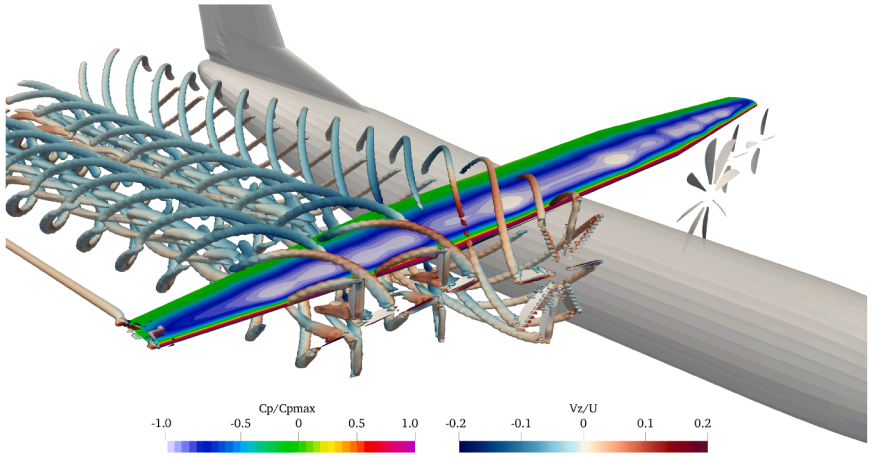

Fig. 12. DUST pressure coefficient distribution and flow visualization with three-dimensional vorticity iso-contours of Q-criterion.

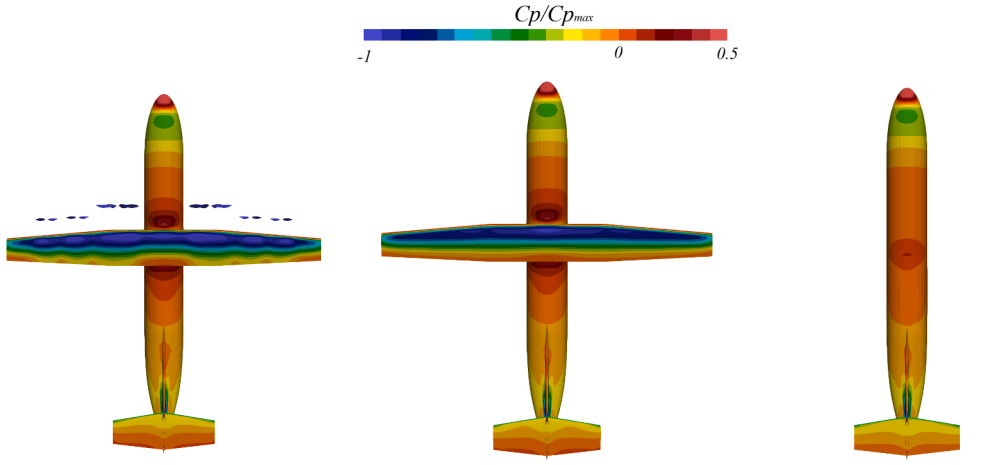

(a) Full with rotors (b) Full without rotors (c) Fuselage-tail

Fig. 13. Pressure coefficient distribution over the entire aircraft for different airplane configuration, at $\alpha = 0°$.

Table 4
Trim optimization problem definition.

Trim Variables	Constraints	Objective
$-2° < \alpha < 9°$ $40° < \theta_{electric} < 60°$ $40° < \theta_{hybrid} < 60°$ $-10° < \delta_e < 10°$	$\sum F_X = 0$ $\sum F_Z = 0$ $\sum m_Y = 0$	L/D ratio

algorithm [53,54], a gradient-based method well suited for nonlinear problems with continuously differentiable objectives and constraints.

In the following discussion, the methodology and selection procedures adopted for the construction of the surrogate models are presented, focusing in this case on the aerodynamic discipline only and following the approach outlined in the introductory section. Fig. 16 shows a sensitivity analysis of the surrogate models, represented through slices of the design hyperspace, highlighting the effect of the size of the training dataset used for the regression model. Gaussian Process Regression (GPR) is employed for surrogate construction. The surrogate model is built using a design-of-experiments approach based on Latin Hypercube Sampling (LHS), which ensures an efficient and uniform sampling of the design space.

As the size of the training dataset increases, the surrogate model progressively converges toward a more stable response, which is subsequently assessed through validation data. This behavior is further quantified in Fig. 17, which reports the convergence of the error metrics as a function of the dataset size, together with the corresponding impact on computational time. Training the surrogate model with 120 samples requires up to 178 min of computational time. The error metrics adopted are those defined in Eq. (1) and show consistent convergence starting from datasets of approximately 60 samples, corresponding to 60 time-marching DUST simulations. The surrogate model selected for use in the MDO framework is therefore trained on 120 samples, as it satisfies the prescribed accuracy requirements of $R_e < 10\%$, $RMSE < 0.1$, and $R^2 > 0.9$ for all outputs of the aerodynamic discipline.

Fig. 18 presents the training points distributed across the design space together with representative slices of the final surrogate model, compared against validation points. Each slice is obtained by varying a single design variable while keeping all others fixed. The figure also reports the distribution of the pointwise relative error computed on the validation dataset, showing that the error remains well below 10% for all outputs of the aerodynamic discipline. As expected, lower errors are observed in regions where the dependence of the output variables on the trim parameters is approximately linear.

Fig. 19 illustrates the sensitivity and coupled dependencies of the same aerodynamic outputs with respect to multiple trim variables simultaneously. In particular, the influence of elevator deflection and angle of attack on aerodynamic loads is highlighted, together with the

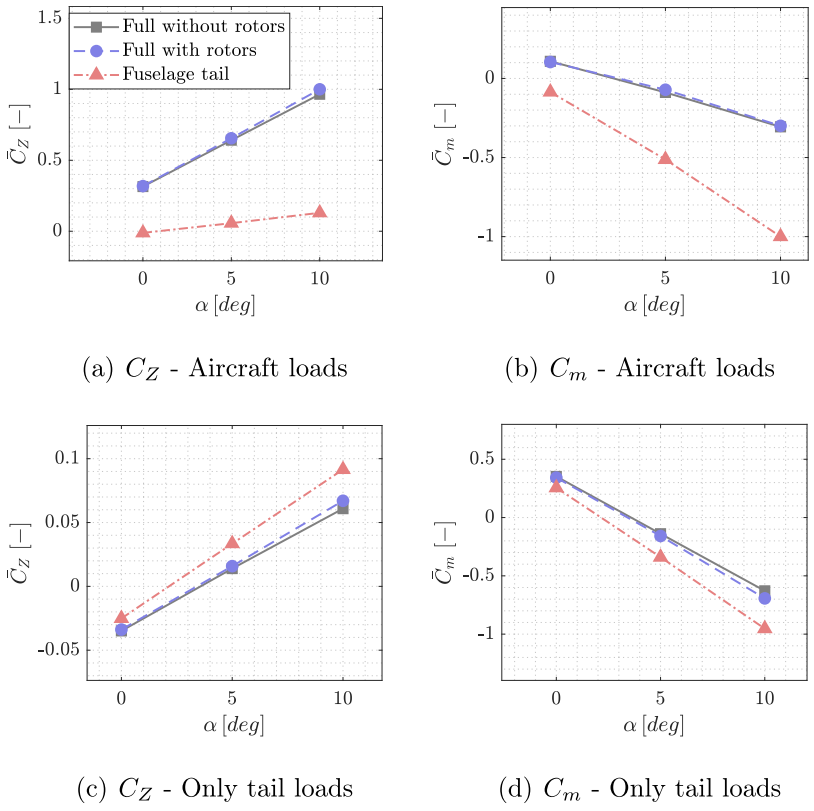

Fig. 14. Body axes integral forces acting over the aircraft configurations.

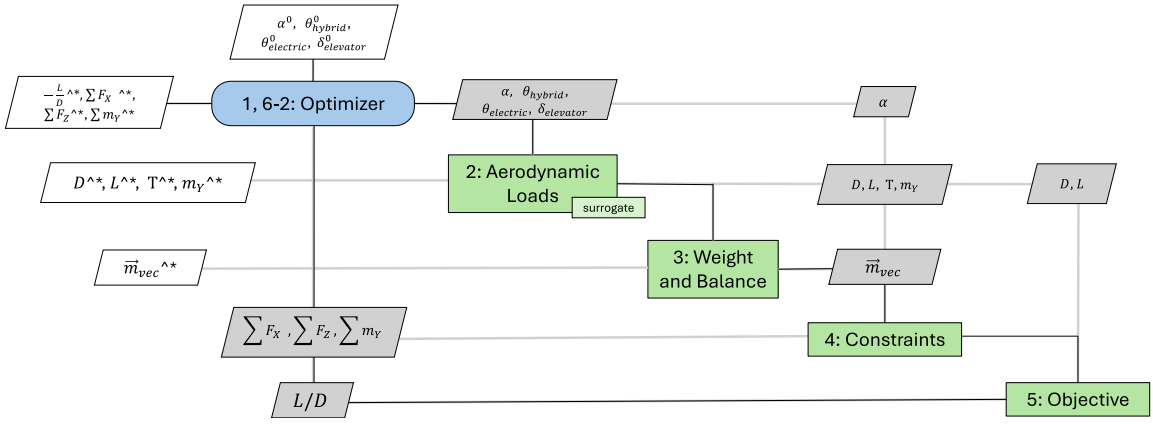

Fig. 15. Extended design structure matrix of the trim problem.

dependence of aircraft thrust on the pitch settings of the hybrid and electric propulsion systems. Surrogate model predictions are again compared with validation points obtained from time-marching simulations performed using DUST.

Table 5 summarizes the surrogate specifications for each aerodynamic output for the employed surrogate, along with accuracy metrics in terms of the coefficient of determination (R^2) and relative error (R_e).

In general, a strong agreement is observed between the surrogate and validation points from time-marching simulations, particularly in terms of trends and derivatives, ensuring consistency with the full-order model. Linear trends such as the lift C_L and pitching moment C_m coefficients achieve higher R^2 values and lower relative errors compared to the more complex drag and thrust coefficients.

Fig. 20 presents the results of the optimization. In particular, the trim condition, defined within a tolerance of 0.05 on the load coefficients, was achieved in 8 iterations. Fig. 20 (a) shows the evolution of the total forces and moments acting on the aircraft across the optimization steps, confirming the convergence toward an equilibrium condition, as well as the convergence criteria employed, i.e. (*i*) a tolerance on objective function f improvement; (*ii*) a relative step-size tolerance on the design variables x_i in the normalized design space; (*iii*) constraint feasibility evaluated through prescribed equality and inequality tolerances;

Table 5
Trim regression final models and accuracy.

	C_L	C_D	C_m	C_t
$n°$ samples	120	120	120	120
Regressor	GPR	GPR	GPR	GPR
R^2 [-]	0.9993	0.9757	0.9979	0.9580
R_e [%]	3.228	7.283	3.841	9.587
$RMSE$ [-]	0.0070	0.0389	0.0051	0.0781

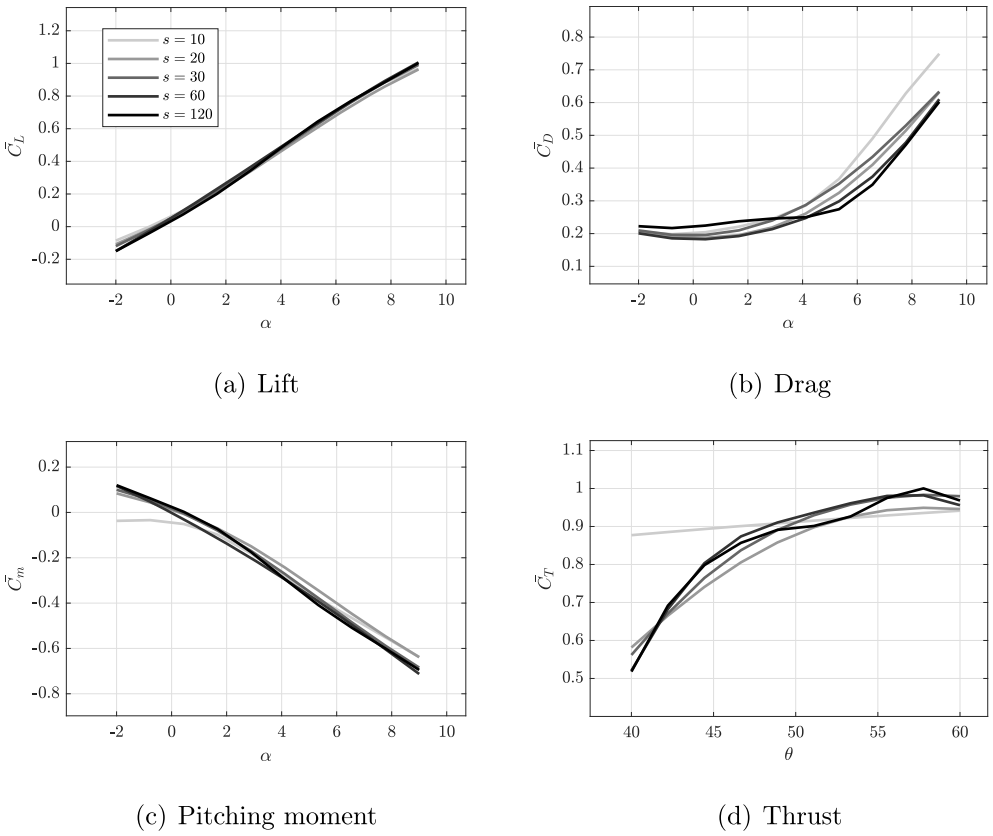

Fig. 16. Surrogate model slices over a single trim variable, convergence study (Increasing dataset/training points size).

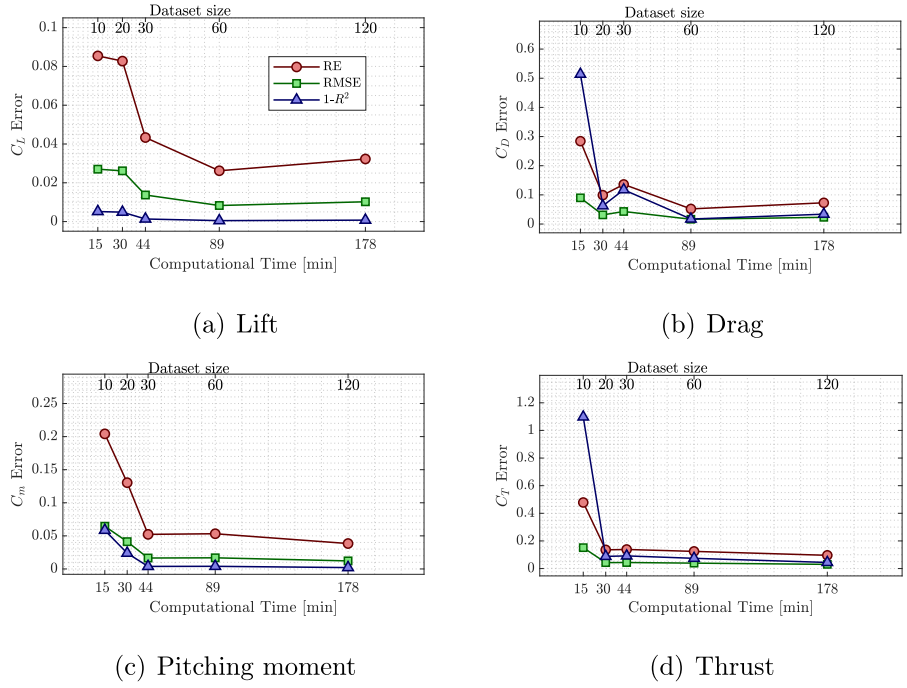

Fig. 17. Surrogate models convergence study, using different error indices. Influence on computational time required for training.

(*iv*) a maximum number of iterations. Fig. 20 shows the evolution of the angle of attack during the optimization, together with the imposed constraint limiting α to the range $[-2°, 9°]$, derived from the aerodynamic validation presented in the previous section. As shown in the figure, the optimized solutions remain comfortably inside the admissible interval throughout the optimization process, never approaching the limits of the validated aerodynamic domain. This confirms both the robustness of the optimization framework and the consistency of the obtained results with the assumptions adopted during the aerodynamic model setup and validation. Fig. 20(c) compares the outcomes of the trim optimization when

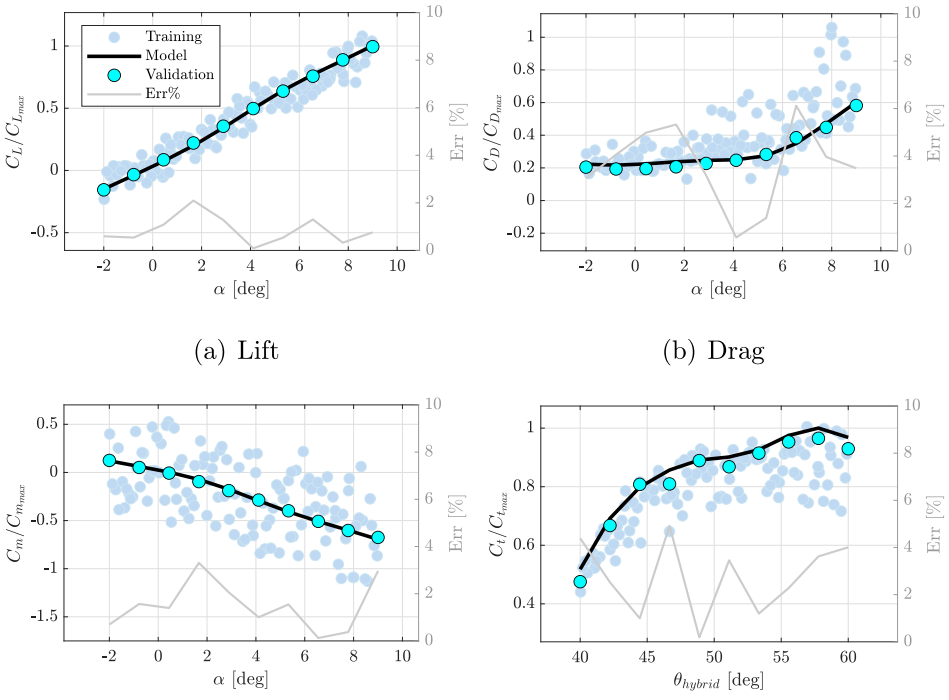

Fig. 18. Slices of the final surrogate models for the aerodynamic discipline outputs: Training data (Dependent on multiple variables), surrogate data with fixed trim variables, validation point with fixed trim variables. Error distribution on validation data.

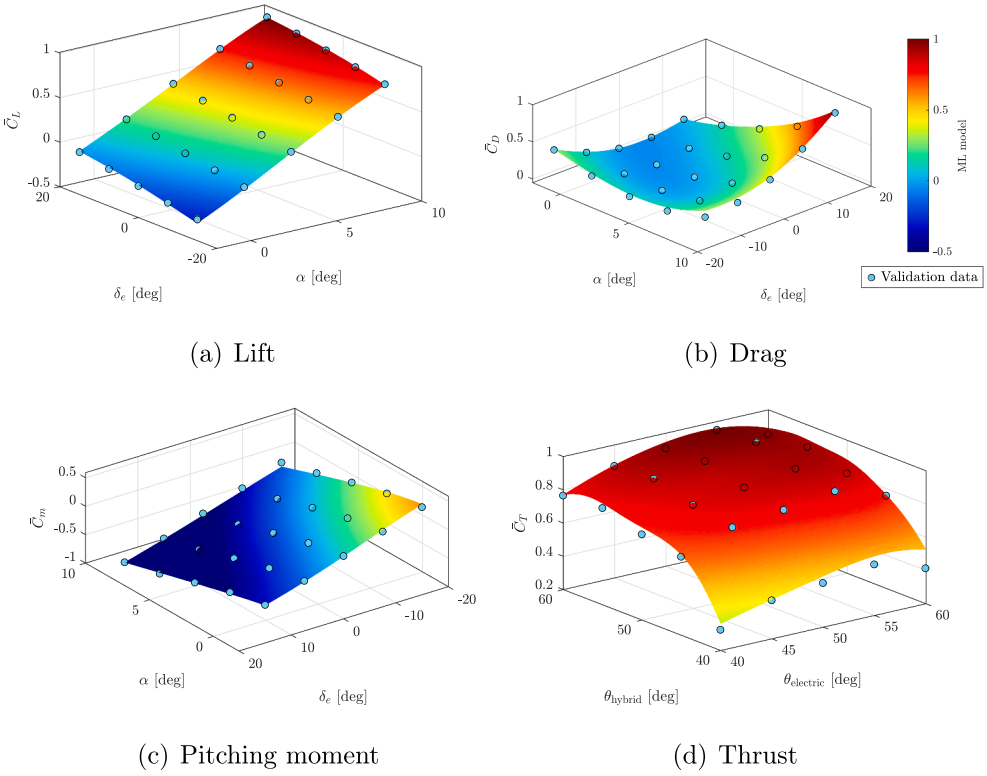

Fig. 19. Final surrogate models for the aerodynamic discipline outputs: Comparison between machine learning model and time-marching simulation validation data.

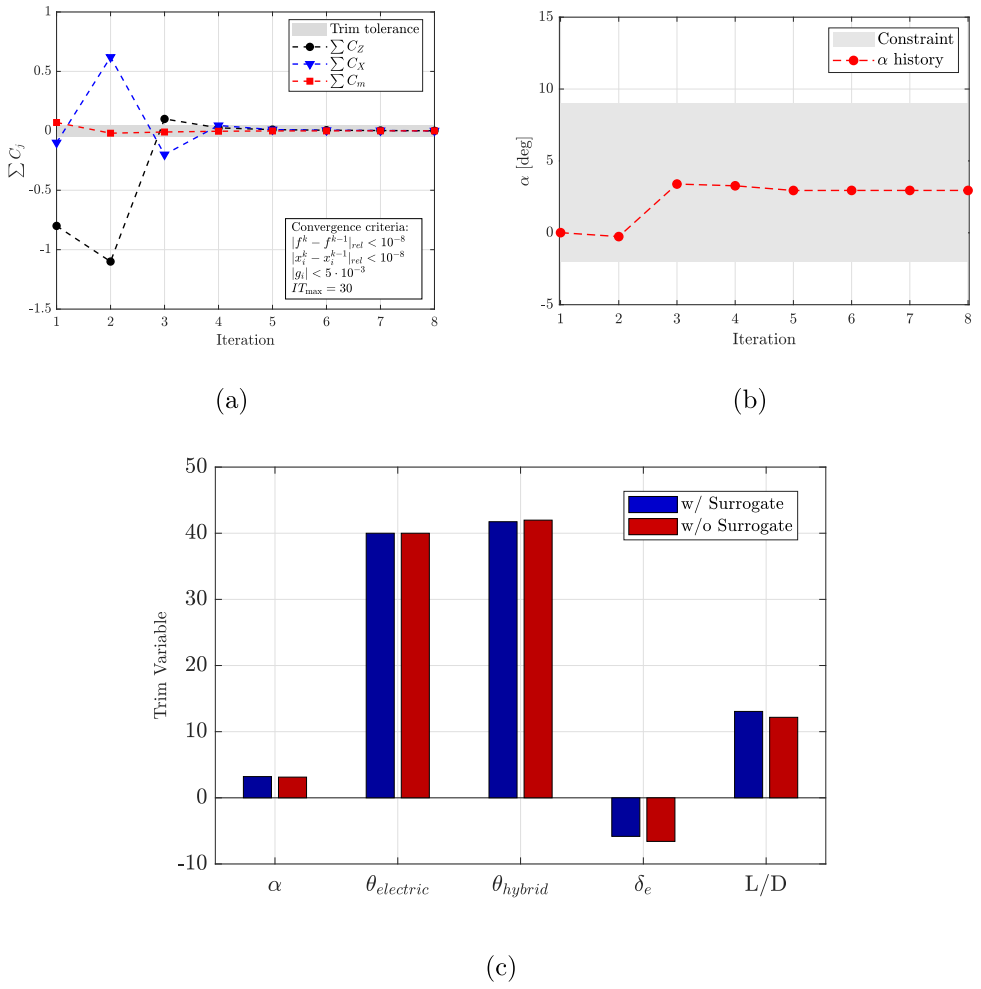

Fig. 20. Comparison of the optimization performance between using the surrogate, and performing time-marching simulation through the optimization: (a) Trim constraints evolution through the optimization and convergence criteria; (b) Angle of attack through optimization; (c) Trim optimization final results.

Table 6
Trim computational time analysis.

$t_{wo/surr}$	t_{train}	$t_{w/surr}$	$tot_{surrogate}$	$\%adv$
4h 34m	4h 16m	0m 1s	4h 16m	-6,57%

Table 7
MDO problem definition.

Design Variables	Constraints	Objective
y_{kink}	$5 < S.M. < 35\%$	Range
θ_{tip}	$2.3 < \omega_{sp} < 3.5\ rad/s$	
y_{eprop}	$0.2 < \zeta_{sp} < 1.4$	
$htail\ scale$	$\zeta_{ph} > 0.04$	
A_{cap}@root	$RFC > 1.5$	
$A_{stringer}$@root	$RFT > 1.5$	

performed with and without the surrogate model for the aerodynamic discipline. A strong correlation between the results is evident, demonstrating the validity and effectiveness of the DOE-based approach and the use of a surrogate model for optimization purposes.

Table 6 shows the computational times associated with each part of the described process. The comparison between trim without surrogates and trim with surrogate training reveals a time advantage of approximately 7%. It is important to highlight that this result is highly dependent on the type of analysis being performed, and that since the trim problem converges in only a few iterations, the benefit of using surrogates is limited. However, once the surrogate is generated, it becomes evident that the exploration of the design space is several orders of magnitude faster compared to using the original discipline.

3.3. Multidisciplinary design optimization with flying qualities constraints

This section presents the results of the MDO performed on the HERA aircraft configuration. Results analysis is focused on two aspects: (i) analysing the effects of introducing or not surrogate models to evaluate the aerodynamic and stability and control behaviour, (ii) the introduction of stability and control constraints in the optimization. Table 7 outlines the definition of the optimization problem, specifically identifying the design variables, constraints, and the objective function. Among the design variables, four are purely geometric, i.e. the wing kink point y_{kink}, the wing tip twist θ_{tip} (twist varies linearly from the airfoil at the kink point), the position of the electric propellers y_{eprop}, which are translated along the wing span while maintaining a constant distance between them (as illustrated in Fig. 21) and finally, the horizontal tail plane scale included in the optimization as a dedicated design parameter to actively control the stability and control characteristics of the aircraft, particularly in response to changes in mass and aerodynamics of the wing that influence the flight dynamics modes. In this context, where flying qualities constraints are incorporated into a multidisciplinary design framework, a global aircraft-level approach is essential, since the evaluation of the complete vehicle dynamics to ensure acceptable flight behavior across the design space is required. As

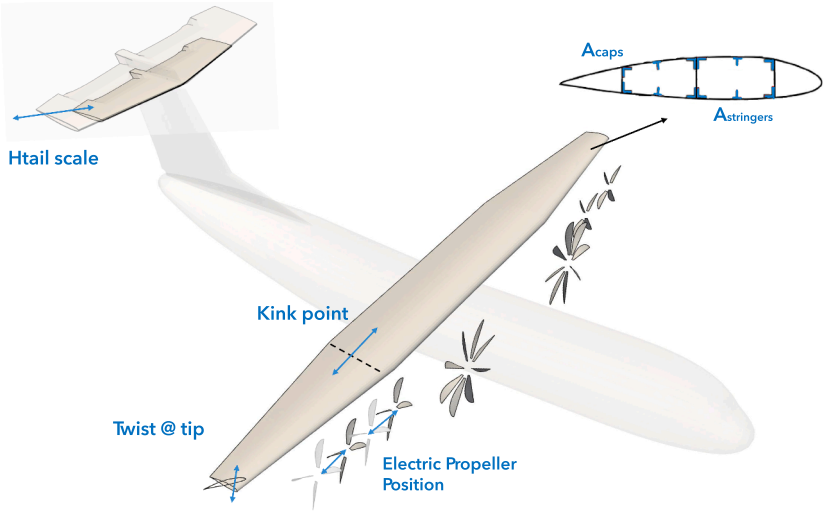

Fig. 21. MDO problem geometric design variables scheme.

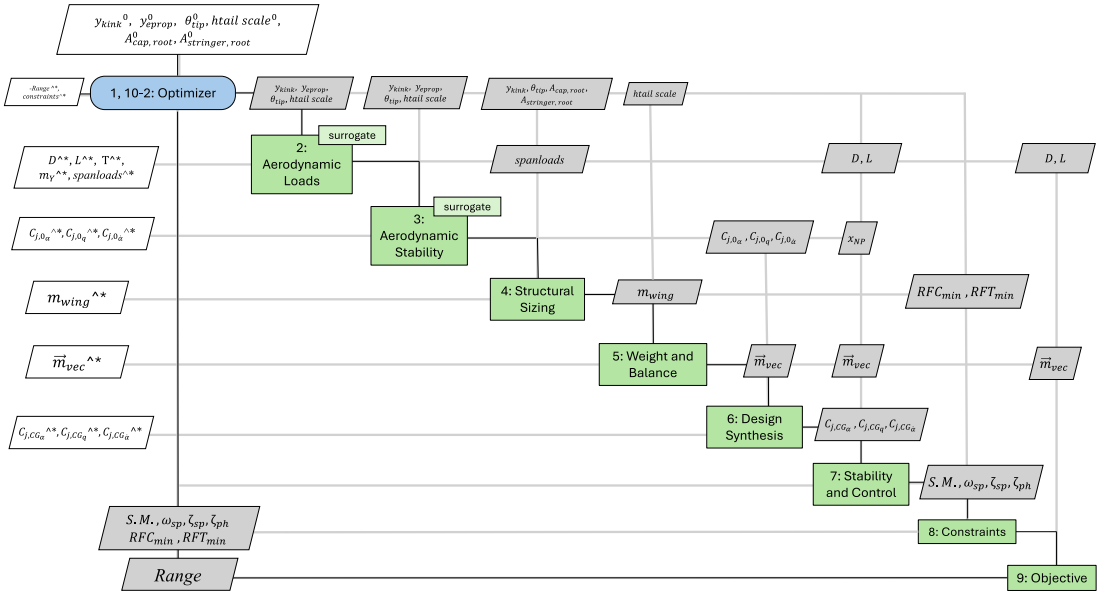

Fig. 22. Extended design structure matrix of the optimization problem.

an assumption of the problem, the wing component center of gravity (CG) is considered fixed, even though its mass variation is accounted for the calculation of the global CG and in the evaluation of the flight dynamics properties. The remaining two design variables pertain to the wing structural geometry, i.e. the area of the caps at the wing root A_{cap} and the area of the stringers $A_{stringer}$. In addition to the upper and lower bounds imposed on the design variables, the optimization includes constraints related to the aircraft's longitudinal flying qualities (FQ). From the perspective of static stability, a constraint is imposed on the aircraft's static margin, defined as:

$$S.M. = \frac{x_{\text{np}} - x_{\text{cg}}}{\bar{c}} = \frac{\frac{-\bar{c}C_{m_\alpha}}{C_{Z_\alpha}} - x_{\text{cg}}}{\bar{c}} = -\frac{C_{m_{CG_\alpha}}}{C_{Z_{CG_\alpha}}} \tag{2}$$

and required to lie between 5% and 35%, to ensure a good compromise between the aircraft's stability and maneuverability. Additional constraints relate to the dynamic behavior of the aircraft, including the damping and frequency of flight mechanics mode (short period and phugoid), derived from a reduced-order model [44] and the stability derivatives obtained using the methodology described in [27]. These constraints are defined as follows:

$$2\zeta_{sp}\omega_{sp} = -\left(\frac{m_{Y_q}}{I_y} - \frac{F_{Z_\alpha}}{Um} + \frac{m_{Y_{\dot{\alpha}}}}{I_y}\right) \tag{3}$$

$$\omega_{sp} = \sqrt{-\frac{m_{Y_q}}{I_y}\frac{F_{Z_\alpha}}{Um} - \frac{m_{Y_{\dot{\alpha}}}}{I_y}} \tag{4}$$

$$\zeta_{ph} = \frac{1}{\sqrt{2}}\frac{C_D}{C_L} \tag{5}$$

The stability and flying qualities constraints are derived from [44] and are based on DEF-STAN 00–970 and MIL-F-8785C, following the established engineering interpretation by Cook [44] selected to be consistent with the weight class and mission profile of the HERA regional aircraft. Specifically, the optimization constraints target Level 1 flying qualities during Category B flight phases (cruise). The short-period requirements follow the limits on the undamped natural frequency ω_s and

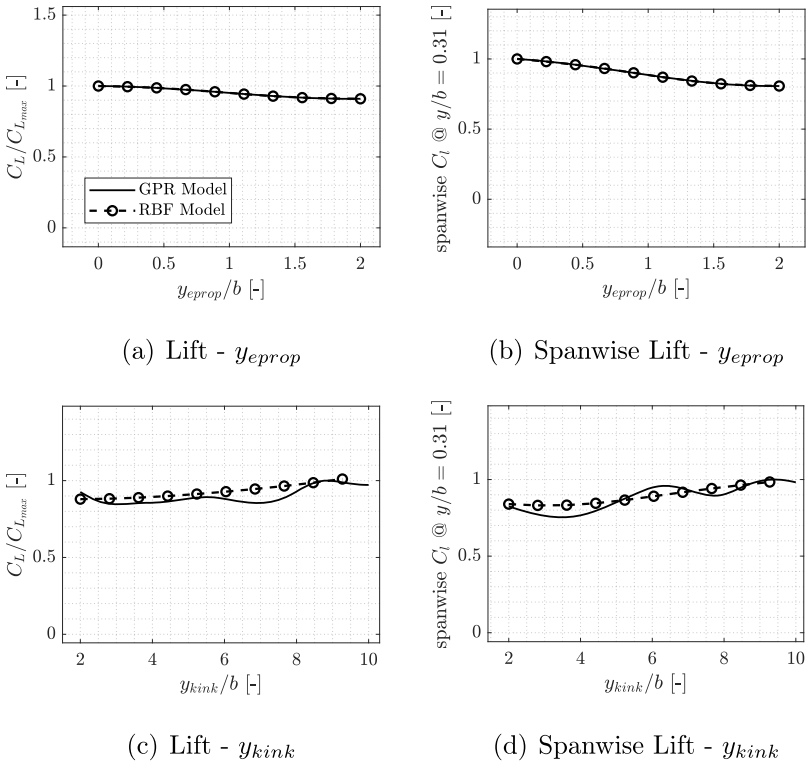

(a) Lift - y_{eprop} (b) Spanwise Lift - y_{eprop}

(c) Lift - y_{kink} (d) Spanwise Lift - y_{kink}

Fig. 23. Slices of surrogate models for the aerodynamic discipline outputs: Comparison between RBF and GPR regressor.

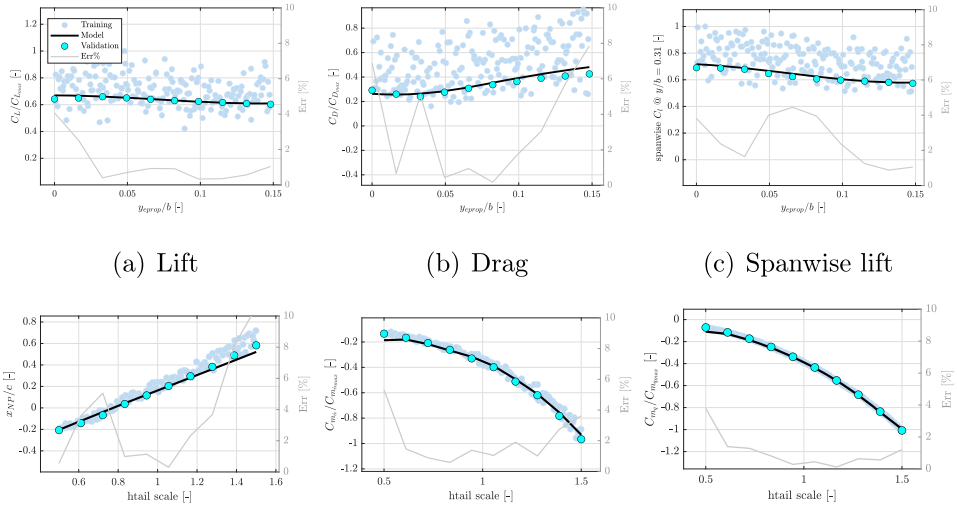

(a) Lift (b) Drag (c) Spanwise lift

(d) A/C Neutral point (e) Plunge derivative (f) Damping in pitch

Fig. 24. Slices of surrogate models for the aerodynamic and stability discipline outputs: Training data (Dependent on multiple variables), surrogate data with fixed design variables, validation point with fixed design variables. Error distribution on validation data.

damping ratio ζ_s, while the phugoid mode follow a minimum damping ratio requirement ζ_p. The choice of these specific numerical thresholds is based on treating the present platform as a Class III aircraft according to the MIL standard classification. For this category of commercial/regional passenger aircraft, ensuring Level 1 dynamics in cruise is a strict requirement to guarantee passenger comfort and safety under autopilot and manual flight. In addition, a static stability requirement is imposed through a constraint on the stability margin, a quantity that represent the ratio between stability and maneuverability. Due to the modular structure of the proposed optimization framework, the same approach can be readily generalized to include additional flying qualities and handling qualities constraints. These may include constraints associated with lateral-directional modes, maneuver-performance metrics such as maneuver response and actuation times, as well as stability and handling qualities requirements for rotorcraft configurations based on ADS-33E specifications.

The last two constraints are related to the structural reserve factors in tension and compression for the structural sizing of the wing [38]. The objective of the optimization is to maximize the aircraft's range, defined by the Breguet range equation:

$$R = \frac{U}{c_s} \cdot \frac{L}{D} \cdot \ln\left(\frac{W_i}{W_f}\right) \tag{6}$$

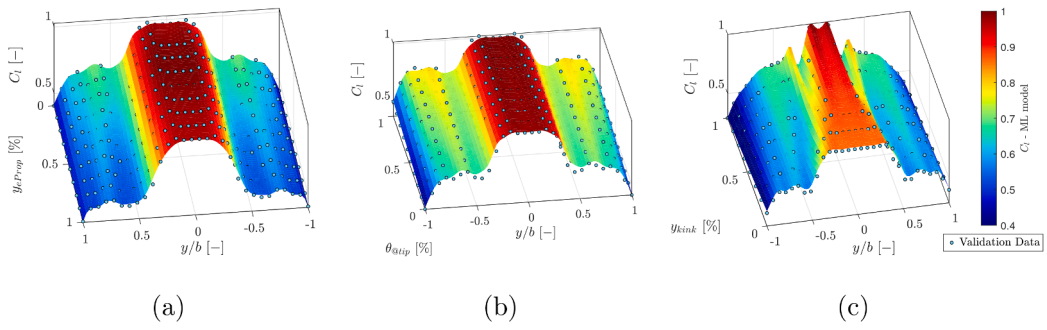

Fig. 25. Spanwise lift surrogate models for the aerodynamic discipline: Comparison between machine learning model and time-marching simulation validation data. C_l dependence with respect to (a) Propeller position; (b) Wing twist @ tip; (c) Wing kink point.

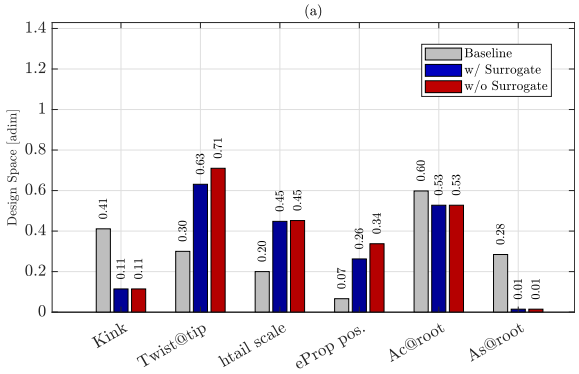

Fig. 26. MDO final results, design variables: Comparison between baseline configuration, optimization with surrogate, and optimization without the surrogate.

Table 8
Optimization regression final models and accuracy.

	C_L	C_D	C_l	x_{NP}	C_{m_α}	C_{m_q}
$n°$ samples	200	200	200	125	125	125
Regressor	RBF	RBF	RBF	GPR	GPR	GPR
R^2 [-]	0.9804	0.9734	0.9841	0.9879	0.9981	0.9992
R_e [%]	3.229	9.452	4.842	8.981	7.470	4.628
$RMSE$ [-]	0.0165	0.0593	0.0165	0.0105	0.0259	0.0252

which provides an optimal balance between maximizing the L/D ratio and minimizing the wing mass.

Fig. 22 presents the XDSM diagram of the optimization problem, showing the inputs (vertical edges) and outputs (horizontal edges) of each discipline. Aerodynamic derivatives are computed in the aircraft's global reference frame, while the design synthesis discipline translates them to the aircraft's center of gravity using outputs from the weight and balance discipline. The optimization is performed using the COBYLA (Constrained Optimization BY Linear Approximations) algorithm, a derivative-free method suitable for constrained and potentially non-differentiable problems [55,56].

Fig. 23 compares the surrogate models generated for the aerodynamic loads discipline using RBF and GPR regressors trained on the same dataset, highlighting that, in this specific case, the GPR model tends to exhibit non-physical overfitting, leading to larger deviations in the predictions. Based on this comparison, the RBF formulation is selected as the most robust and consistent surrogate for the aerodynamic loads discipline. Fig. 24 presents the surrogate models generated by the framework, namely a RBF regressor for the aerodynamic loads discipline trained on 200 sampled points and a GPR regressor for the aerodynamic stability discipline trained on 120 points. Both models use Latin Hypercubic sampling for the generative DOE. This choice also provides a general indication that the final surrogate model selection is driven by a trade-off between accuracy and available training data, ensuring the best compromise between number of sampled points and computational cost (see Tables 8 and 9). Therefore, in the present activity, the surrogate selection has been performed by evaluating the best-fitting model for a given dataset, i.e., the model that minimizes prediction errors for a fixed number of training samples.

Table 8 summarizes the surrogate specifications for each output variable, together with the corresponding R^2 and mean relative error R_e. A strong correlation between surrogate predictions and validation points is observed for both disciplines. For the aerodynamic loads discipline, the response surfaces exhibit relatively low gradients and greater dispersion, resulting in slightly higher errors and reflecting the limited sensitivity of C_L, C_D, and C_m to the design variables. Nevertheless, all coefficients achieve $R^2 > 0.97$ with mean R_e below 10.

The aerodynamic stability discipline, in contrast, shows a strong dependence on the horizontal tail scaling parameter, which dominates the response of the stability derivatives. This leads to reduced dispersion and higher accuracy, with R^2 values exceeding 0.99 and relative errors comparable to or lower than those of the load models. Fig. 25 illustrates representative trends for the aircraft neutral point x_{NP} and the dynamic stability derivatives $C_{m_{\dot\alpha}}$ and C_{m_q}, computed by DUST using the methodology described in [27].

Fig. 25 also presents the surrogate model of the sectional load distribution, which is an output of the aerodynamic discipline, together with its dependence on the wing design variables, in comparison with the validation points corresponding to the spanwise load directly computed by DUST. Once again, a good correlation is observed between the machine-learning-based surrogate model and the DUST results, with limited discrepancies in regions characterized by higher gradients, while the overall topology predicted by the aerodynamic solver is consistently preserved.

Fig. 26 presents the MDO optimization results in terms of design variables and objectives, highlighting solutions that satisfy the constraints

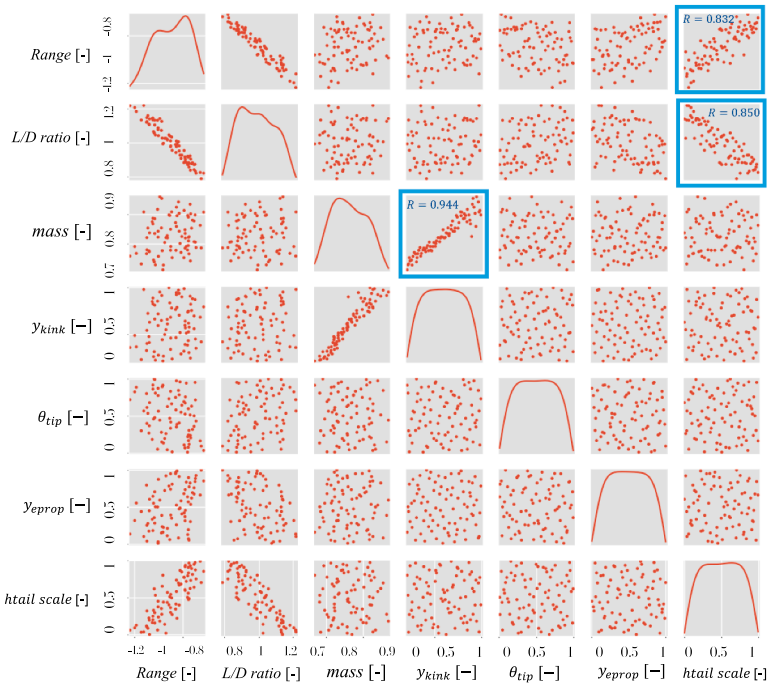

(a) Objective f - Design Var. x_i

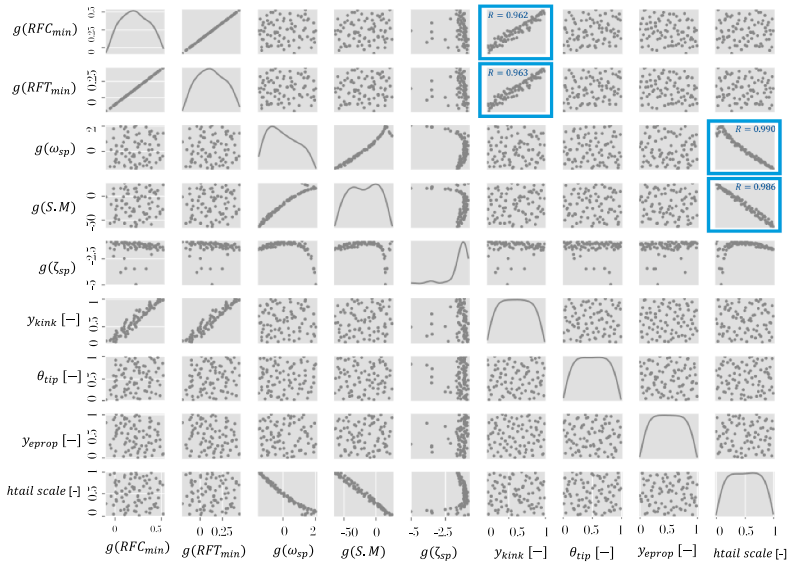

(b) Constraint g - Design Var. x_i

Fig. 27. Scatter plot matrix created from a 120 design of experiment highlighting (a) Dependence of the objective variables with respect to the design variables; (b) Dependence of the constraint expressions with respect to the design variables. Relevant correlations are highlighted in blue. Variables are represented as non-dimensionalized with respect to the design space. (For interpretation of the references to colour in this figure legend, the reader is referred to the web version of this article.)

on flying qualities. A good agreement is observed between results obtained with and without surrogate models, confirming the consistency of the DOE-based approach.

In particular, Fig. 26(a) shows the geometric and structural design variables normalized to the relative design space, where 0 corresponds to the lower bound and 1 to the upper bound. Key geometric changes compared to the HERA UCB baseline include a kink point y_{kink} shifted toward the wing root, an increase in tip twist θ_{tip}, and a larger horizontal tail scale, with increments of 30.0%, 41.3%, and 25.2%, respectively. The propeller position y_{eprop} moves outward from 20.0% to 45.2% of the wing span. Considering aerodynamic performance, this outward shift improves the wing L/D ratio, though it increases the bending moment due to engine weight. Structural optimization shows a 7% reduction in spar cap area, while stringer areas reach the lower limit of the

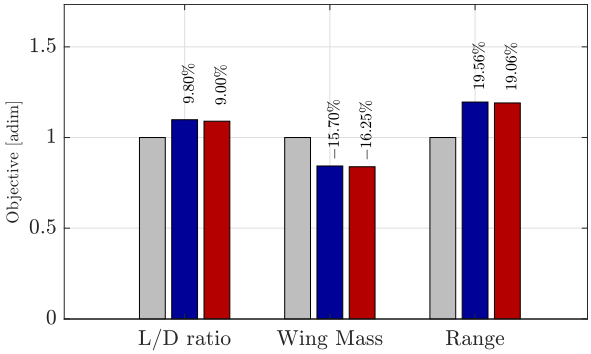

Fig. 28. MDO final results, objectives: Comparison between baseline configuration, optimization with surrogate, and optimization without the surrogate.

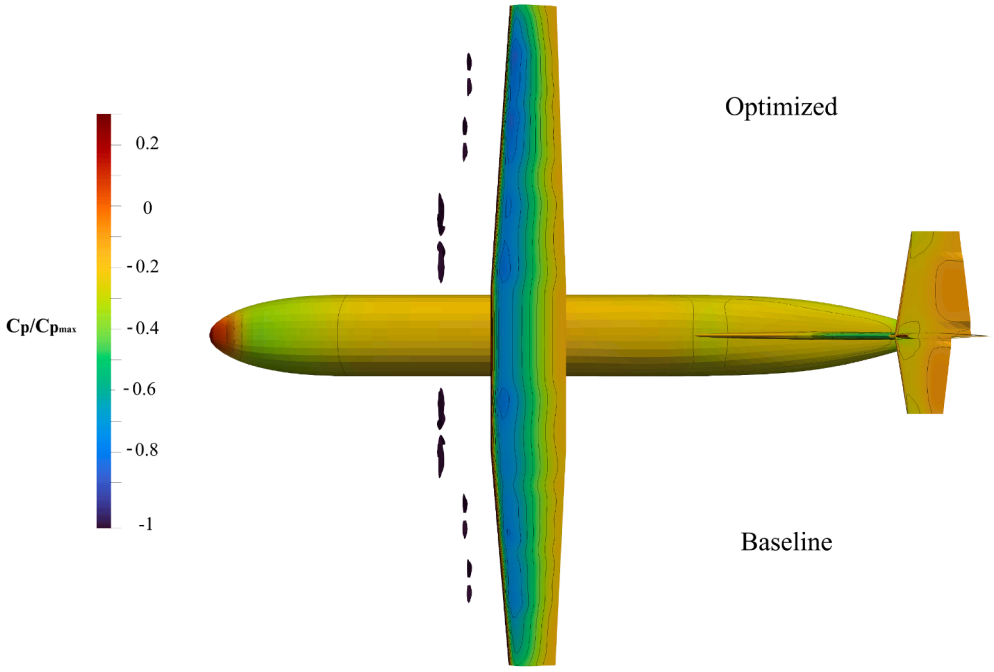

Fig. 29. Optimization results: Comparison of the pressure coefficient distribution and geometry between the optimized and baseline aircraft configuration.

design space. The largest deviations between surrogate and full-order results occur in wing tip twist and propeller position. To investigate the source of these discrepancies, a detailed sensitivity analysis was performed by analyzing scatter plot matrices obtained over a 120 samples Design of Experiment (DoE) relating the design variables to both the objective functions (see Fig. 27(a)) and the optimization constraints (see Fig. 27(b)). These plots clearly highlight that y_{eprop} and the wingtip twist angle exhibit a significantly lower sensitivity compared to the remaining design variables. This reflects a sparse design space region, which naturally leads to lower correlation levels (below $R = 0.9$) and a higher prediction error range, quantified at approximately 8% for these specific parameters. This behavior therefore explains the poorer correlation observed for these two variables in the comparison between the surrogate-based predictions and the time-marching model results. Despite this local discrepancy, the global consistency between the surrogate models and the high-fidelity results remains robust. This behavior is a coherent consequence of the obtained global performance of the surrogate models (as illustrated in Figs. 24 and 25), which maintain a low average prediction error of about 3-4%.

Fig. 28 shows the comparison of the objectives L/D ratio, wing mass, and range. The optimization leads to a 9.0% increase in L/D, a 16.25% reduction in wing mass, and a 19.06% increase in range, consistent with the Breguet range equation. Deviations between surrogate and non-surrogate results are minimal, i.e. 0.80%, 0.55%, and 0.50% for L/D, wing mass, and range, respectively.

In order to highlight the main differences in terms of aircraft configuration led by the optimization, Fig. 29 shows a mirrored (with respect to longitudinal plane of the aircraft) visualization of the pressure coefficient distribution on the aircraft, as well as the geometrical comparison between the optimized and baseline configuration.

Fig. 30(a) illustrates the optimization path of the aircraft range over the iterations, as well as the convergence criteria employed, and showing similar trajectories for optimizations with and without surrogates, confirming the reliability of the surrogate-based approach. Fig. 30(b) presents a Pareto front obtained by minimizing wing mass while incrementally constraining L/D, normalized to baseline values. The original range-oriented optimization selects a point on the Pareto optimal front, achieving a balance between wing mass reduction and L/D increase. The comparison between surrogate and full-order evaluations shows very small deviations, i.e. 0.55% and 0.179% for mass, 0.80% and 0.183% for L/D.

Table 9 reports computational times for optimizations with and without surrogates, including surrogate training. Four surrogate models were used, i.e. one for aerodynamic loads and three for aerodynamic stability derivatives, each trained separately due to the need for dedicated simulations [52]. The total optimization time with surrogates, including

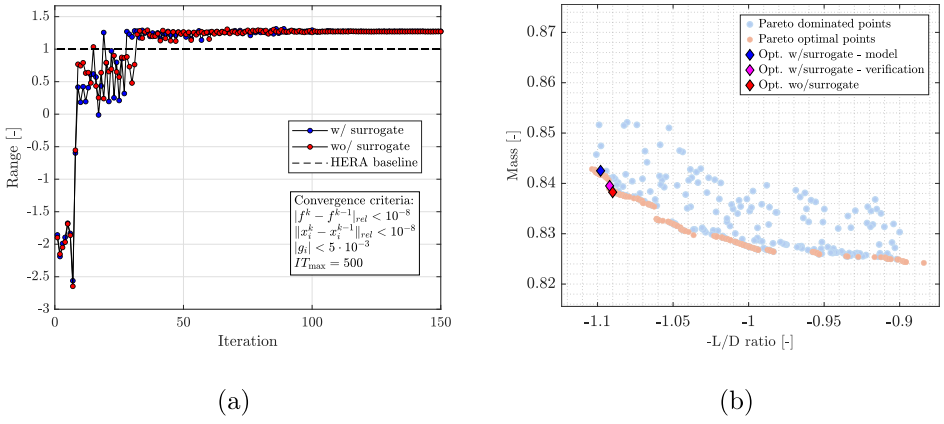

Fig. 30. (a) Objective function convergence and convergence criteria; (b) Mass-L/D ratio Pareto optimal front, and optimized configuration predicted with and without surrogate model for aerodynamic loads.

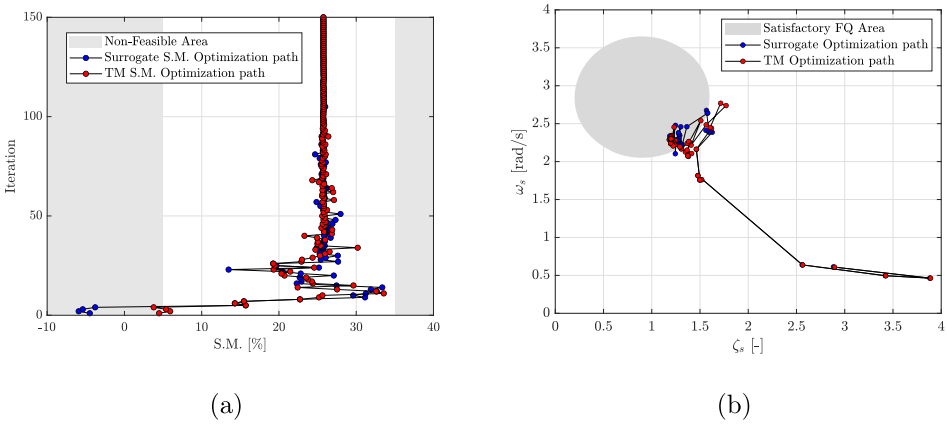

Fig. 31. (a) Static margin constraint optimization history. Surrogate and time marching (TM) comparison. (b) Short period constraint on the finger-print short-period flying qualities graph.

Table 9
Optimization computational time.

$t_{wo/surr}$	t_{train}		$t_{w/surr}$	$tot_{surrogate}$	$\%adv$
66h 15m	Aero loads	6h 40m	4m 55s	32h 28m	-49.01%
	Static C_{l_α}	13h 19m			
	Plunge $C_{l_{\dot{\alpha}}}$	6h 12m			
	Phugoid C_{l_q}	6h 12m			

training, is approximately 49% of the time required without surrogates, while maintaining accuracy (see Fig. 25 and Table 8). The computational advantage is greater than in the trim problem due to the larger number of iterations needed for convergence.

Fig. 31(a) shows the evolution of the constraint on the static stability margin of the aircraft, expressed as the percentage difference between the neutral point of the aircraft and the center of gravity, which are both varying within the optimization history. It is shown that the implemented framework can effectively consider this constraint while optimizing the configuration. The optimization path for the static margins (SM) is predominantly driven by the horizontal tail scale design variable, which plays a major role in determining the static stability characteristics of the aircraft (see Fig. 25), while the influence of the variation of the mass and aerodynamic properties of the wing has a secondary effect. The SM enters the feasibility region relatively early in the optimization loop, showing that it is effectively controlled by the parametrization on the tail plane scale. The comparison between the behaviour of the optimizer with surrogates and with time marching simulations (TM) is again very similar, highlighting the potentiality of the approach.

Fig. 31(b) illustrates the evolution of the short-period mode frequency and damping ratio constraints throughout the optimization process. In particular, the constraint boundaries adopted from [44], derived from DEF-STAN 00–970 and MIL-F-8785C flying qualities requirements, are superimposed onto the so-called fingerprint graph. As discussed by Cook, this diagram identifies the region in the $\omega_s - \zeta_s$ plane corresponding to combinations of natural frequency and damping ratio that have been assessed through pilot evaluations as providing satisfactory flying qualities. The resulting representation therefore allows both verification that the optimization framework is capable of handling dynamic flying qualities constraints effectively, and confirmation that the optimized configurations converge toward the desired region of acceptable short-period dynamic behavior in terms of frequency and damping characteristics.

Within this satisfactory region, the aircraft demonstrates adequate maneuverability (initial response) without excessive sensitivity to control inputs, and its oscillations remain well damped. It can be observed that, during the optimization, the applied constraint drives the aerodynamic and mass properties of the aircraft toward this favorable FQ region. The horizontal tail scale emerges as the primary factor influencing the short period characteristics (see m_{Y_α} in Eq. (4)), while modifications to the main wing mass and aerodynamic properties provide secondary effects.

4. Conclusion

This work presents the application of a multi-disciplinary design and optimization (MDO) framework to the Clean Aviation HERA UCB configuration, addressing the strong couplings between aerodynamics,

structures, propulsion, and stability that characterize hybrid-electric regional aircraft with distributed electric propulsion (DEP). The framework, built around GEMSEO, integrates DUST-based aerodynamic models and explicitly incorporates stability, control, and trim requirements as design constraints, enabling a comprehensive and modular approach to aero-structural optimization.

DUST aerodynamic model was validated against RANS simulations from the TAU solver. Later in order to reduce the computational cost associated with mid-fidelity simulations, surrogate models were developed using supervised machine learning regression and a design of experiments (DOE) methodology, forming a multi-fidelity optimization strategy.

Using the developed framework, longitudinal trim and aero-structural optimization were performed, targeting maximization of aircraft range while minimizing wing mass and improving aerodynamic efficiency. The results demonstrate strong agreement between surrogate-based predictions and high-fidelity simulations, both in terms of design variables and objective functions, highlighting the accuracy of the reduced-order models. The methodology successfully enforces flying qualities and stability constraints, ensuring that the optimized configuration meets the desired performance across trimmed flight conditions.

Overall, this study confirms that the extended MDO framework provides a robust and efficient tool for the design of complex hybrid-electric aircraft. By combining modular integration of disciplines, multi-fidelity optimization, and machine learning-based surrogate modeling, it enables reliable exploration of trade-offs between aerodynamic efficiency, structural weight, and flight stability, supporting informed and effective design decisions.

Future research will focus on extending the framework to an integrated full-aircraft optimization incorporating the geometric and structural design variables of the fuselage, which are currently kept fixed. Such an advancement will require the integration of higher-fidelity aerodynamic tools to properly capture the complex flow fields and aerodynamic efficiency variations associated with fuselage shape modifications. Moreover, another interesting open point to be investigated is a more rigorous characterization of surrogate error ranges by integrating formal uncertainty quantification (UQ) methodologies into the multidisciplinary optimization framework.

CRediT authorship contribution statement

D. Granata: Writing – original draft, Visualization, Validation, Software, Methodology, Investigation, Formal analysis, Data curation, Conceptualization; **S. Mancini:** Writing – original draft, Supervision, Software, Methodology, Investigation, Data curation, Conceptualization; **A. Mateo-Gabin:** Writing – original draft, Software, Methodology, Investigation, Formal analysis; **A. Zanotti:** Writing – review & editing, Writing – original draft, Supervision, Resources, Project administration, Methodology, Investigation, Funding acquisition, Conceptualization.

Data availability

The authors do not have permission to share data.

Declaration of competing interest

The authors declare that they have no known competing financial interests or personal relationships that could have appeared to influence the work reported in this paper.

Acknowledgements

This project has received funding from the Clean Aviation Joint Undertaking under the European Union's Horizon Europe research and innovation programme under Grant Agreement HERA (Hybrid-Electric Regional Architecture) n° 101102007. Views and opinions expressed are however those of the author(s) only and do not necessarily reflect those of the European Union or CAJU. Neither the European Union nor the granting authority can be held responsible. The authors thank Jose Fernandez Montes for his valuable support in the integration of the structural sizing discipline and Sven Lanzan Ferran for the feedback on the multidisciplinary design framework. Thanks to Daniela Gisele Francois from DLR for the support on the TAU setup.

Daniele Granata would like to thank the support by PNRR 118 - TDA, Cycle 39 - Transitions (Ministerial Decree 118/23), funded by the European Union - Next Generation EU, Mission 4 Component 1. CUP: D43C23002740001

References

[1] W. Johnson, C. Silva, NASA concept vehicles and the engineering of advanced air mobility aircraft, Aeronaut. J. 126 (1295) (2022) 59–91.
[2] Hydrogen-powered aviation: A fact-based study of hydrogen technology, economics, and climate impact by 2050, https://www.clean-aviation.eu/media/publications/hydrogen-powered-aviation-report.
[3] HERA – hybrid electric regional architecture project, https://project-hera.eu/.
[4] M.T. Fard, J. He, H. Huang, Y. Cao, Aircraft distributed electric propulsion technologies-a review, IEEE Trans. Transp. Electrif. 8 (4) (2022) 4067–4090.
[5] J. Wu, F. Gao, S. Li, F. Yang, Conceptual design and optimization of distributed electric propulsion general aviation aircraft, Aerospace 10 (5) (2023) 387.
[6] H.D. Kim, A.T. Perry, P.J. Ansell, A review of distributed electric propulsion concepts for air vehicle technology, in: 2018 AIAA/IEEE Electric Aircraft Technologies Symposium (EATS), IEEE, 2018, pp. 1–21.
[7] J.W. Lim, Fundamental investigation of proprotor and wing interactions in tiltrotor aircraft, in: Proceedings of the 75th Annual Vertical Flight Society Forum and Technology Display, Philadelphia, PA, USA, 2019, pp. 13–16.
[8] A. Savino, A. Cocco, A. Zanotti, V. Muscarello, et al., Numerical investigation of wing-propeller aerodynamic interaction through a vortex particle-based aerodynamic solver, in: 48th European Rotorcraft Forum (ERF 2022), Curran, 2022, pp. 1–9.
[9] A. Zanotti, L. Menini, A. Savino, D. Grassi, L. Riccobene, Experimental investigation of wing-propeller aerodynamic interaction in eVTOL configurations, Aerosp. Sci. Technol. 152 (2024) 109348.
[10] C. Niro, A. Savino, A. Cocco, A. Zanotti, Mid-fidelity numerical approach for the investigation of wing-propeller aerodynamic interaction, Aerosp. Sci. Technol. 108950 (2024).
[11] G. Qiao, G.N. Barakos, Aerodynamic study of wingtip-mounted propeller and distributed propulsion system, in: Proceedings of the 49th European Rotorcraft Forum (ERF), Rotterdam, The Netherlands, 2024.
[12] N. Böhnisch, C. Braun, P. Marzocca, V. Muscarello, Insights into the aeroelastic stability of a wing with distributed electric propulsion systems, Aerosp. Sci. Technol. 168 (2025) 110763.
[13] E. Santos, A. Serena, S. Claverías, F. Arévalo, H. Climent, M. Karpel, Aeroelastic challenges in the clean aviation hybrid-electric regional aircraft, in: Proceedings of the International Forum of Aeroelasticity and Structural Dynamics (IFASD), The Hague, The Netherlands, 2024.
[14] G. Grazioso, M. Di Stasio, F. Nicolosi, S. Trepiccione, A mathematical model for hybrid-electric propulsion system for regional propeller-driven aircraft, Energy Convers. Manag. X 26 (2025) 100957.
[15] F. Volle, Aero-structural optimization of the AIAA MDO benchmark model with TAU and lagrange, in: AIAA SCITECH 2025 Forum, 2025, p. 2815.
[16] A. Mateo-Gabín, T. Wagenaar, S. Mancini, J. Florenciano Merino, S. Lanzan Ferran, Analysis and optimization of a distributed propulsion system for a regional transport aircraft, in: ECCOMASS 2024 Congress, 2024.
[17] A.A. Giunta, O. Golividov, D.L. Knill, B. Grossman, W.H. Mason, L.T. Watson, R.T. Haftka, Multidisciplinary design optimization of advanced aircraft configurations, in: Fifteenth International Conference on Numerical Methods in Fluid Dynamics: Proceedings of the Conference Held in Monterey, CA, USA, 24–28 June 1996, Springer, 2007, pp. 14–34.

[18] V. Trifari, Development of a multi-disciplinary analysis and optimization framework and applications for innovative efficient regional aircraft, Phd Univ. Naples Federico II Dep. Ind. Eng. Univ. Naples Federico II Naples Italy (2020).
[19] M.R. Setayandeh, A.-R. Babaei, Multidisciplinary design optimization of an aircraft by using knowledge-based systems, Soft Comput. 24 (16) (2020) 12429–12448.
[20] E.S. Hendricks, E. Aretskin-Hariton, D. Ingraham, J.S. Gray, S.L. Schnulo, J. Chin, R. Falck, D. Hall, Multidisciplinary optimization of an electric quadrotor urban air mobility aircraft, in: AIAA Aviation 2020 Forum, 2020, p. 3176.
[21] Ö. Petersson, F. Daoud, Multidisciplinary Optimization of Aircraft Structures with Respect to Static and Dynamic Aeroelastic Requirements, Deutsche Gesellschaft für Luft-und Raumfahrt-Lilienthal-Oberth eV, 2012.
[22] A. Gazaix, F. Gallard, V. Ambert, D. Guénot, M. Hamadi, S. Grihon, P. Sarouille, T.Y. Druot, J. Brézillon, V. Gachelin, et al., Industrial application of an advanced bi-level MDO formulation to aircraft engine pylon optimization, in: AIAA Aviation 2019 Forum, 2019, p. 3109.
[23] K.R. Moore, A. Ning, Distributed electric propulsion effects on existing aircraft through multidisciplinary optimization, in: 2018 AIAA/ASCE/AHS/ASC Structures, Structural Dynamics, and Materials Conference, 2018, p. 1652.
[24] M.A. Clarke, R.M. Erhard, J.T. Smart, J. Alonso, Aerodynamic optimization of wing-mounted propeller configurations for distributed electric propulsion architectures, in: AIAA Aviation 2021 Forum, 2021, p. 2471.
[25] S. Biser, M. Filipenko, M. Boll, N. Kastner, G. Atanasov, M. Hepperle, D. Keller, D. Vechtel, M. Noe, Design space exploration study and optimization of a distributed turbo-electric propulsion system for a regional passenger aircraft, in: 2020 AIAA/IEEE Electric Aircraft Technologies Symposium (EATS), IEEE, 2020, pp. 1–27.
[26] D. Planas Andrés, E. Nguyen Van, C. Döll, P. Pastor, Multi-disciplinary optimization of a distributed electric propulsion aircraft under aero-propulsive effects, CEAS Aeronaut. J. 16 (2) (2025) 571–589.
[27] D. Granata, A. Savino, A. Zanotti, Numerical evaluation of aircraft aerodynamic static and dynamic stability derivatives by a mid-fidelity approach, Aerospace 11 (3) (2024) 213.
[28] C. Bonaventura, A. Guardone, Mid-fidelity aerodynamic analysis and design of a fixed-wing eVTOL for the martian atmosphere, in: AIAA Aviation Forum and Ascend 2025, 2025, p. 3015.
[29] N.T. Frink, B.R. Hiller, P.C. Murphy, K. Cunningham, G.H. Shah, Investigation of reduced-order modeling for aircraft stability and control prediction, in: AIAA Scitech 2019 Forum, 2019, p. 0980.
[30] Politecnico di Milano, https://www.dust.polimi.it/.
[31] GEMSEO Documentation, GEMSEO: generic engine for multi-disciplinary scenarios, exploration, and optimization, https://gemseo.readthedocs.io/en/stable/index.html#.
[32] M. Tugnoli, D. Montagnani, M. Syal, G. Droandi, A. Zanotti, Mid-fidelity approach to aerodynamic simulations of unconventional VTOL aircraft configurations, Aerosp. Sci. Technol. 115 (2021) 106804.
[33] DLR, TAU, https://www.dlr.de/en/as/research-and-transfer/software-solutions/aerodynamics/software-tau.
[34] A. Savino, A. Cocco, A. Zanotti, M. Tugnoli, P. Masarati, V. Muscarello, Coupling mid-fidelity aerodynamics and multibody dynamics for the aeroelastic analysis of rotary-wing vehicles, Energies 14 (21) (2021) 6979.
[35] B.B. Hillier, M.J. Stock, A. Gharakhani, Robust and corrected coefficients for the ROtor-body-INteraction body, AIAA J. 59 (10) (2021) 4281–4283.
[36] P.D. Gray, NeuralFoil - a neural network-based airfoil performance predictor, 2023, https://github.com/peterdsharpe/AeroSandbox.
[37] A. Mateo-Gabín, T. Wagenaar, S. Mancini, et al., Analysis and optimization of a distributed propulsion system for a regional transport aircraft, in: 9th European Congress on Cimputational Methods in Applied Sciencies and Engineering (ECCOMAS 2024), 2024, pp. 1–13.
[38] A. Mateo, M.A. Martín, J. Fernandez, S.A.L. Ferran, S. Mancini, T. Klaproth, An AI-Enhanced Multidisciplinary Optimization Framework for Net-Zero Transport Aircraft, https://doi.org/10.2514/6.2025-3293
[39] DLR, CPACS, https://dlr-sl.github.io/cpacs-website.
[40] W. Johnson, NDARC NASA Design and Analysis of Rotorcraft: Theory, Technical Report, National Aeronautics and Space Administration, 2025.
[41] J.F. Montes, Optimización de Parámetros de Ala-Mediante Algoritmos Genéticos, Universidad Politécnica de Madrid, Madrid, 2015.
[42] A. Mateo-Gabín, S. Mancini, M.A. Martín, J. Fernández Montes, S.A. Lanzan Ferran, T. Klaproth, An AI-enhanced multidisciplinary optimization framework for net-zero transport aircraft, in: AIAA 2025, Las Vegas, 2025, pp. 1–18.
[43] A. Mateo, A.M. Marta, J. Fernandez, S.A. Lanzan Ferran, S. Mancini, T. Klaproth, An AI-enhanced multidisciplinary optimization framework for net-zero transport aircraft, in: AIAA Aviation Forum and Ascend 2025, 2025, p. 3293.
[44] M.V. Cook, Flight Dynamics Principles: A Linear Systems Approach to Aircraft Stability and Control, Butterworth-Heinemann, 2012.
[45] A. Savino, Multi-fidelity aerodynamic optimization of the wing extension of a tiltrotor aircraft, Appl. Sci. 15 (17) (2025) 9491.
[46] D.C. Montgomery, Design and Analysis of Experiments, John wiley & sons, 2017.
[47] J. Fang, G. Sun, N. Qiu, N.H. Kim, Q. Li, On design optimization for structural crashworthiness and its state of the art, Struct. Multidiscip. Optim. 55 (2017) 1091–1119.
[48] J.C. Helton, F.J. Davis, Latin hypercube sampling and the propagation of uncertainty in analyses of complex systems, Reliab. Eng. Syst. Saf. 81 (1) (2003) 23–69.
[49] C. Williams, C. Rasmussen, Gaussian processes for regression, Adv. Neural Inf. Process. Syst. 8 (1995) 514-520.
[50] Y. Wu, H. Wang, B. Zhang, K.-L. Du, Using radial basis function networks for function approximation and classification, Int. Sch. Res. Not. 2012 (1) (2012) 324194.
[51] S.A. Tran, J.W. Lim, Interactional aerodynamics of the XV-15 tiltrotor aircraft during conversion maneuvers, J. Am. Helicopter Soc. 67 (3) (2022) 56–68.
[52] D. Granata, A. Savino, A. Zanotti, Evaluation of a mid-fidelity approach for the calculation of tiltrotor aerodynamic stability derivatives in cruise flight conditions, Aerosp. Sci. Technol. 164 (2025) 110384.
[53] D. Kraft, A software package for sequential quadratic programming, Forschungsbericht- Dtsch. Forsch.- Vers. fur Luft- Raumfahrt (1988).
[54] D. Kraft, Algorithm 733: TOMP–fortran modules for optimal control calculations, ACM Trans. Math. Softw. 20 (3) (1994) 262–281.
[55] M.J.D. Powell, A direct search optimization method that models the objective and constraint functions by linear interpolation, in: Advances in Optimization and Numerical Analysis, Springer, 1994, pp. 51–67.
[56] M.J.D. Powell, Direct search algorithms for optimization calculations, Acta Numer. 7 (1998) 287–336.